On the role of the Antarctic Slope Front on the occurrence of the Weddell Sea Polynya under climate change.

Joseph Lockwood

Masters of Science

Atmospheric and Oceanic Sciences

McGill University

Montreal,Quebec

2020-03-16

A thesis submitted to the Faculty of Graduate Studies and Research in partial fulfillment of the requirements for the degree of Master of Science

ACKNOWLEDGEMENTS

I acknowledge the support provided by the McGill University Stephen and Anastasia Mysak Graduate Fellowship in Atmospheric and Oceanic Sciences. I would like to thank Professor Lawrence Mysak for his generosity, which enabled me to carry out my masters under privileged conditions. I am also grateful to my supervisor, Professor Carolina Dufour, for all her help and support. I acknowledge the support I received from Natural Sciences and Engineering Research Council of Canada (NSERC). I was also supported by Québec Océan's Short training support program. I thank Alexander Haumann, Graeme MacGilchrist and Casimir de Lavergne for helpful comments and discussions on this study. I would also like to thank Dany Dumont for reviewing the manuscript. I thank the CMIP5 archive and NASA for providing access to the LLC_4320 model data.

ABSTRACT

This study investigates the occurrence of the Weddell Sea Polynya (WSP) under an idealized climate change scenario by evaluating simulations from climate models of different ocean resolutions. The GFDL-CM2.6 climate model, with roughly 3.8 km horizontal ocean grid spacing in the high latitudes, forms a WSP at similar time and duration under idealized climate change forcing as under pre-industrial forcing. In contrast, all convective models forming the fifth phase of the Coupled Model Intercomparison Project (CMIP5) show either a cessation or a slowdown of WSP events under climate warming. The representation of the Antarctic Slope Current and related Antarctic Slope Front is found to be key in explaining the differences between the two categories of models, with these features being of realistic strength in CM2.6, yet weak and/or missing in CMIP5 models. In CM2.6, the freshwater input driven by sea ice melt and enhanced runoff found under climate warming largely remains on the shelf region since the slope front restricts the lateral spread of the freshwater. In contrast, for most CMIP5 models, open ocean stratification is enhanced by the freshening since the absence of a slope front allows coastal freshening to spread into the open ocean, thus resulting in a slow down in the occurrence of WSPs. Hence, poor representation of Weddell Sea shelf processes in CMIP5 models might affect the ability of these models to predict the fate of the WSPs under climate change.

ABRÉGÉ

Cette thèse examine la récurrence de la polynie de la mer de Weddell (WSP) dans un contexte de changement climatique à l'aide de modèles de climat de résolutions différentes dans l'océan. Dans le modèle de climat du GFDL CM2.6, d'une résolution horizontale de 3.8 km aux hautes latitudes, une WSP apparaît avec un timing et une durée similaires dans un scénario de contrôle pré-industriel et dans un scénario idéalisé de changement climatique. À l'inverse, parmi les modèles climatiques participant à la phase 5 du Projet d'intercomparaison de modèles couplés (CMIP5), tous ceux qui présentent des épisodes réguliers de convection aux hautes latitudes montrent soit un arrêt complet, soit un espacement des événements de WSP en réponse au changement climatique. Il est montré que la représentation du courant de talus continental antarctique (ASC) et du front qui lui est associé (ASF), est à l'origine de la différence de réponse entre ces deux catégories de modèles. Si les ASC et ASF sont représentés de manière réaliste dans CM2.6, ils sont de faible intensité, voire même absents, dans les modèles CMIP5. Dans CM2.6, l'eau douce en provenance de la fonte de la banquise ainsi que des apports continentaux accrus en raison du changement climatique, reste principalement dans la région du plateau continental en raison de la présence de l'ASF qui empêche toute propagation de cette eau douce vers le large. Au contraire, dans la grande majorité des modèles CMIP5, la stratification dans les régions hauturières est intensifiée par cet apport d'eau douce qui peut se propager vers le large en raison de l'absence d'ASF, entraînant ainsi une apparition plus rare de la WSP. Aussi, la représentation médiocre des processus dynamiques dans la région du plateau continental en mer de Weddell pourrait entraver la capacité des modèles CMIP5 à prédire le devenir des WSPs dans une période de changement climatique.

CONTRIBUTION OF AUTHORS

This thesis is based on a co-authored manuscript: J. Lockwood, C.O. Dufour, S. M. Griffies, M.Winton; On the role of the Antarctic Slope Front on the occurrence of the Weddell Sea polynya under climate change, submitted to the *Journal of Climate* in February 2020. J. Lockwood completed the analysis of all model simulations and wrote the original manuscript. C.O. Dufour conceived the study and contributed to the interpretation of the results and writing of the original manuscript. S. M. Griffies and M.Winton contributed to the interpretation of the results and provided edits to the manuscripts. The thesis and paper manuscript differ from each other as the thesis has the addition of Section 1-1 of the Introduction. Furthermore, Figures 1-1, 1-2, 2-1 and 3-14 only appear in the thesis version and all supplementary material of the paper has been included in the text of the thesis.

TABLE OF CONTENTS

LIST OF TABLES

LIST OF FIGURES

1
Introduction

1.1 Polynyas

Polynyas are regions of open ocean enclosed in sea ice ranging in area from 10 to 10^5 km^2. When spatially defined on one side by the coast, these open ocean areas are called coastal polynyas (e.g., North Water Polynya), whereas when bounded by land-fast ice they are called flaw polynyas (e.g. Laptev Sea Polynya). Whilst predominately formed in coastal regions, polynyas can form in the open ocean such as within Antarctic pack ice. Polynyas are sites of strong ocean-atmosphere moisture and heat exchange, with the newly open ocean effecting freshwater and momentum balances (Comiso and Gordon, 1987).

Polynyas are often classified according to the means of formation; either through latent heat or sensible heat mechanisms. Latent heat polynyas are mechanically driven and are created in areas where ice motion is divergent due to stress imparted by the prevailing winds or oceanic currents (Fig. 1–1; Morales Maqueda et al. 2004). Sensible heat polynyas are thermally driven, formed when the flux of heat from the deep ocean to the ocean surface is sufficient in both melting existing sea ice and suppress the formation of new ice. In latent heat polynyas, heat loss to the atmosphere across the air-sea interface induces a feedback such that ice is continually generated in the polynya region before being laterally advected. Theses polynyas thus are areas of high sea ice production (Morales Maqueda et al., 2004). Sensible heat polynyas depend on the flux of heat to the upper ocean and their size is therefore determined by the amount of heat advected to the surface. As a result, sensible heat polynyas are often areas of low sea ice production. This classification though can be seen as over-simplified as the formation of a polynya often modifies the original physical forcing through feedback mechanisms (Melling et al., 2001). The conditions that create a latent heat polynya, for example, promote upwelling and mixing, which can bring sensible heat to the surface.

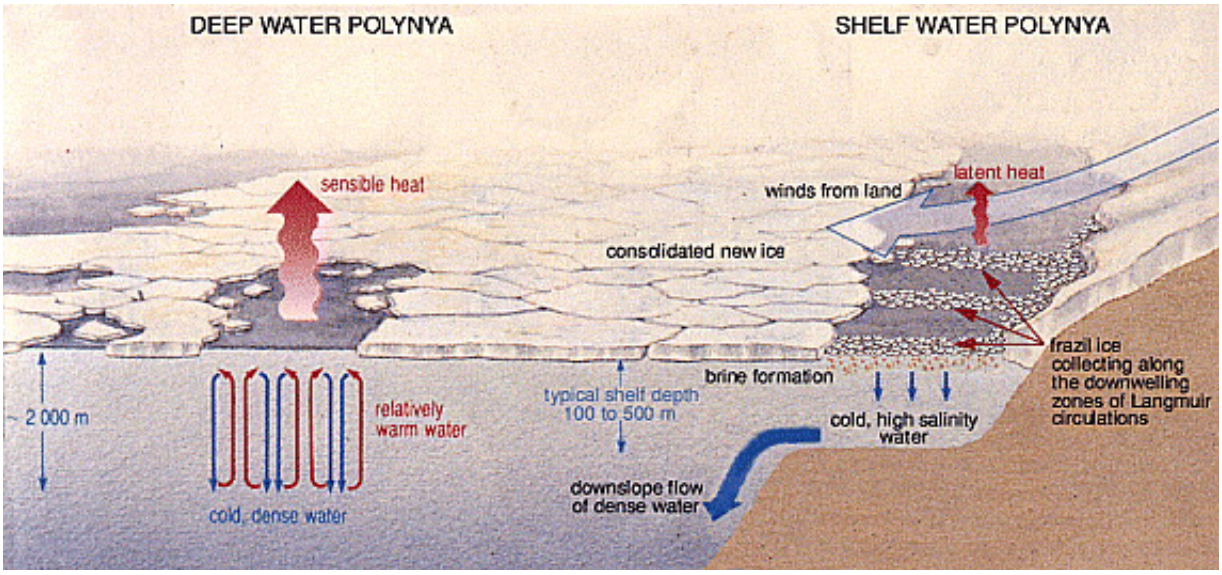

Figure 1–1: Schematic diagram of sensible heat and latent heat polynyas and associated physical processes. Source; Morales Maqueda et al. (2004).

1.2 The Weddell Sea Polynya

Over the winters of 1974 to 1976, satellite observations from the Nimbus-5 Electrically Scanning Microwave Radiometer revealed the presence of a large polynya within the Antarctic pack ice of the Weddell Sea (Carsey, 1980), covering an estimated average area of 250×10^3 km^2 (Gordon et al., 2007). This polynya, known as the Weddell Sea Polynya (WSP; Fig. 1–2), was maintained by intense vertical convection of warm water from depth (Martinson et al., 1981). The heat responsible for the formation of the polynya was advected from a subsurface heat reservoir (SHR) located in the Weddell Deep Water in the Weddell Sea. The SHR is identified by a water column temperature maximum between 0 - 1.3°C in the depth range of approximately 130 to 1600 m (Smedsrud, 2005). During convection, this warm water was directly exposed to the atmosphere. This process induced a buoyancy exchange such that the newly exposed water cooled, releasing heat to the atmosphere, before subsequently sinking back to the deep ocean and forming intense chimneys of convection extending down to 3000 m (Gordon, 1978). The upward flux of heat during convection and subsequent cooling at depth is thought to have contributed to the formation of the Antarctic Bottom Water (AABW) for the following decade, thus acting to intensify global ocean overturning circulation. Observational estimates from Gordon (1982) suggest that deep water enhancement during the WSP was between 1.6 - 3.2 Sv (Sv = 10^6 m^3 s^{-1}). In addition, reconstructions of the

air-sea interaction associated with this polynya suggest large localized atmospheric perturbations with ocean-to-atmosphere moisture and heat losses causing +20°C surface (2 m) air temperature anomalies and 50% higher cloud cover over the polynya during several months of 1976 compared to climatology (Moore et al., 2002).

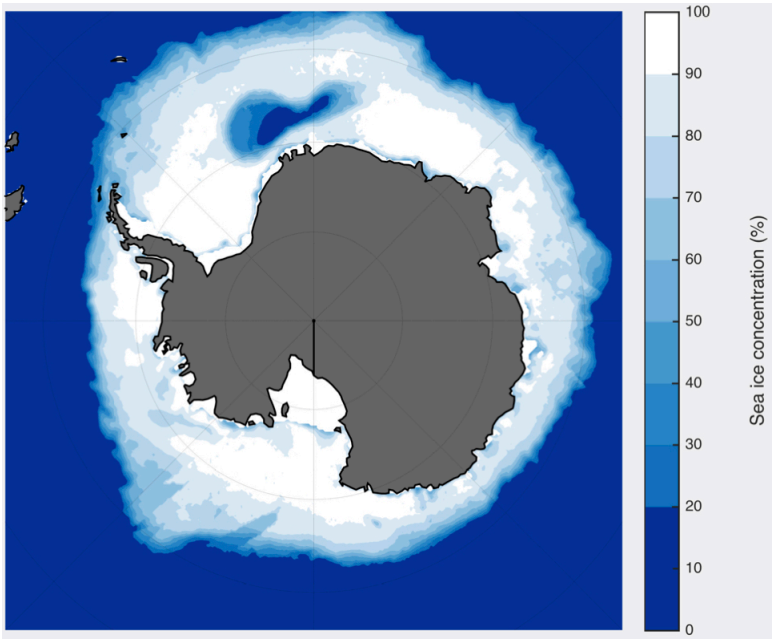

Figure 1–2: Observed 1974–1976 mean September sea ice concentration (%) from Nimbus-5 ESMR Polar Gridded Sea Ice Concentrations delineating the Weddell Polynya extent (Parkinson, 2014).

Since the initial observation of the WSP in the 1970s, a number of mechanisms have been proposed that may have overcome the regionally weak salinity stratification, thus initiating the convection events. These mechanisms include intense surface cooling and brine rejection during sea ice formation (Martinson et al., 1981), enhanced horizontal cyclonic oceanic eddy activity (Holland, 2001) and Taylor column circulation (Kurtakoti et al., 2018) at the Maud Rise. A transition of the Southern Annular Mode (SAM) from a prolonged negative phase to a positive phase may have also contributed to the formation of the WSP, with negative phases resulting in high surface salinity anomalies due to drier and colder surface conditions (Gordon et al., 2007) and positive phases resulting in a strengthening of the Southern Hemisphere westerlies, the combination of which initiate convection (Cheon et al., 2014). Once initiated, deep convection will have continued until

either the depletion of the SHR (Martin et al., 2013) or input of freshwater to the surface (Comiso and Gordon, 1987), both of which will have re-established water column stability.

The occurrence of a similar polynya in the Weddell Sea region was not observed again until the winters of 2016 and 2017, when a large sea ice hole opened over the Maud Rise (Campbell et al., 2019; Jena et al., 2019). Despite being the largest polynya observed at the Maud Rise since 1980 (Cheon and Gordon, 2019), these polynyas were substantially smaller compared to the 1970's WSP, stabilizing at approximately 50×10^3 km^2 ($\approx$20% of the 1970's WSP) between September and November 2017 (Jena et al., 2019). Unlike the 1970's WSP which propagated westward from the Maud Rise into the open ocean at an average velocity of 0.013 m s^{-1}, this recent event remained at the Maud Rise. Analyses of observations over the winters of 2016 and 2017 have suggested that this event was preconditioned by wind-driven upwelling that weakened the haline stratification (Campbell et al., 2019; Cheon and Gordon, 2019). The initiation of these events have been linked to the passage of severe cyclones causing sea ice divergence and turbulent mixing (Campbell et al., 2019; Francis et al., 2019). Enhanced poleward meridional transport of heat and moisture, associated with an amplification of the atmospheric zonal wave-3 and a strong positive SAM index, may have contributed to polynya formation over these winters (Francis et al., 2019). Wind induced spin-up of the cyclonic Weddell Gyre and strong negative wind curl over the Maud Rise are also suggested to have led to the formation of the 2017 polynya (Cheon and Gordon, 2019).

1.3 Weddell Sea Polynya in models

Among the fifth phase of the Coupled Model Intercomparison Project (CMIP5) models, deep ocean convection is common in the Southern Ocean under pre-industrial simulations (de Lavergne et al., 2014), although these events are often categorized as spurious as most models overestimate spatial extent compared to observations (Heuzé et al., 2013). AABW formation in CMIP5 models is primarily controlled by these convection events, as coastal processes leading to the formation and cascading of dense shelf waters down the continental slope are not resolved in these relatively coarse resolution models ($\approx 1°$). CMIP5 models, therefore, often exhibit biases in Southern Ocean

water mass properties and stratification (Heywood et al., 2014), as well as in their representation of large scale ocean dynamics such as the Antarctic Circumpolar Current (Beadling et al. 2019).

Recent studies utilizing models with relatively fine ocean horizontal grid spacing ($\leq$ 1 km) have allowed for the investigation of finer scale processes in the Southern Ocean. These models have revealed that mesoscale eddies support a significant transport of heat and mass across the Antarctic Slope Front (ASF; Stewart and Thompson 2015), a front present in most regions of Antarctica that presents a strong barrier to tracer transport (Thompson et al., 2018). The inability of CMIP5 models to capture the dynamics on the shelf and fine scale processes in that region may result in biases in the mean state circulation and water mass properties, in turn impacting climate change projections. Notably, under climate change simulations, open-ocean convection in CMIP5 models has been reported to slow down, and associated polynyas to occur less frequently or even cease, owing to enhanced upper ocean stratification (de Lavergne et al., 2014). In contrast, our analysis of the Geophysical Fluid Dynamics Laboratory (GFDL) CM2.6 global climate model, with an ocean component of 0.1° horizontal grid spacing ($\approx$ 3.8 km at 70°S) reveals a continuation of convection events and of the WSP under a climate change simulation (Section 3.1). Considering the atmospheric and oceanic changes brought about by polynya formation, an accurate representation of convection and polynya formation in the Southern Ocean is required to ensure reliable model projections of regional and global climate. Understanding the physical mechanisms accounting for the different behavior found in CM2.6 versus CMIP5 is the goal of this paper.

1.4 Overview

Our hypothesis is that, because of their relatively coarse ocean resolutions, the CMIP5 models are unable to represent important processes involved in the formation of polynyas and in their response to climate change. To investigate this hypothesis, we use pre-industrial control (piControl) and idealized 1% yr^{-1} carbon dioxide (CO_2) rise (1pctCO_2) simulations of CM2.6 and of CMIP5 models to investigate the response of the WSP to climate change (Section 2). We first compare the occurrence of open-ocean deep convection and WSP events in the models under the piControl and 1pctCO_2 simulations (Section 3.1). We find a strong relationship between convection events,

surface salinity and vertical density stratification under climate change (Section 3.2), and a freshening at the surface which is driven by enhanced runoff and sea ice change (Section 3.3.1). In CM2.6, the spatial distribution of freshening is predominately confined to the coasts through the effects of the Antarctic Slope Current (ASC) and Antarctic Slope Front (ASF; Section 3.3.2). In Section 4.1, we evaluate the ability of CM2.6 and CMIP5 models to represent the ASF and ASC by comparing them to the ultra-fine resolution LLC_4320 model (1/48° horizontal grid spacing; Rocha et al. 2016). Although CM2.6 lacks certain of the fine scale features found in LLC_4320, this model-model comparison shows that CM2.6 provides a more realistic representation of the ASF and ASC than CMIP5 models.

2
Methods

2.1 Models

2.1.1 The GFDL CM2.6 climate model

The GFDL CM2.6 climate model, which is part of the GFDL CM2-O climate model, is the key tool for this study (Delworth et al., 2012; Griffies et al., 2015). CM2.6 has a horizontal atmospheric grid spacing of 0.45° with 32 vertical levels formulated on a cubed-sphere grid, in which the atmosphere is represented on the six sides of a cube. CM2.6's ocean component uses version 5 of the Modular Ocean Model (MOM5; Griffies et al. 2015) with volume-conserving Boussinesq kinematics. The horizontal grid is tri-polar, with two poles in the northern hemisphere and one at the South Pole (Murray, 1996). The vertical grid has 50 levels with thicknesses of 10 m at the surface increasing with depth to 210 m. CM2.6 has a horizontal ocean grid spacing of 0.10°, corresponding to a grid size of 3.8 km at 70° S. CM2.6 is an eddy rich model at mid latitudes, notably in the Antarctic Circumpolar Current (Delworth et al., 2012; Griffies et al., 2015), and therefore does not employ a mesoscale eddy parameterization. However, CM2.6 does not fully resolve mesoscale eddies on high latitude continental shelves which requires roughly a 1 km horizontal resolution (St-Laurent et al. 2013; Hallberg 2013). Sea ice is simulated by the GFDL Sea Ice Simulator (SIS) which is a dynamical model with three vertical layers, one snow and two ice, and five ice-thickness categories (Winton, 2000). The sea ice model uses the same horizontal tripolar grid as the ocean component.

Vertical mixing in CM2.6 is determined by the K-profile parameterization (KPP) scheme (Large et al., 1994). Within this boundary layer, the turbulent mixing is parameterized using a nonlocal bulk Richardson number. Below the boundary layer, vertical mixing is parameterized through the local gradient Richardson number. The Fox-Kemper et al. (2011) parameterization is employed to represent submesoscale mixed layer eddies. Regions of gravitational instability are stabilized by enhanced vertical diffusivity and viscosity (Klinger et al., 1996). A description of the

representation of the Southern Ocean and Antarctic coasts in CM2.6 can be found in Griffies et al. (2015); Dufour et al. (2017) and Goddard et al. (2017). Note that CM2.6 has a high transient climate response, defined as the year 61–80 average global warming of the 1pctCO_2 experiment, of 2°K (Winton et al., 2014).

2.1.2 CMIP5 models

CMIP5 models comprise a range of climate models and Earth System Models, differing from each other in terms of model structure, including vertical coordinate, grid resolution and subgrid parameterizations (Taylor et al., 2012). We analysed all CMIP5 models for which the following monthly output were available for the investigated experiments (see Section 2.1.4): sea ice concentration (sic), potential temperature (thetao) and salinity (so). The resulting 23 CMIP5 models used in this study have horizontal ocean grid spacing generally $\geq 1°$ (Fig. 2–1). Due to their relatively coarse ocean resolution, the transport and mixing by mesoscale eddies are parameterized in the CMIP5 models. Some processes representative of surface waves and tides are taken into account in the parameterization of vertical mixing in a number of CMIP5 models used. The full list of models used in this study, along with horizontal grid spacings and treatment of oceanic gravitational instabilities, is available in Table. 2–1.

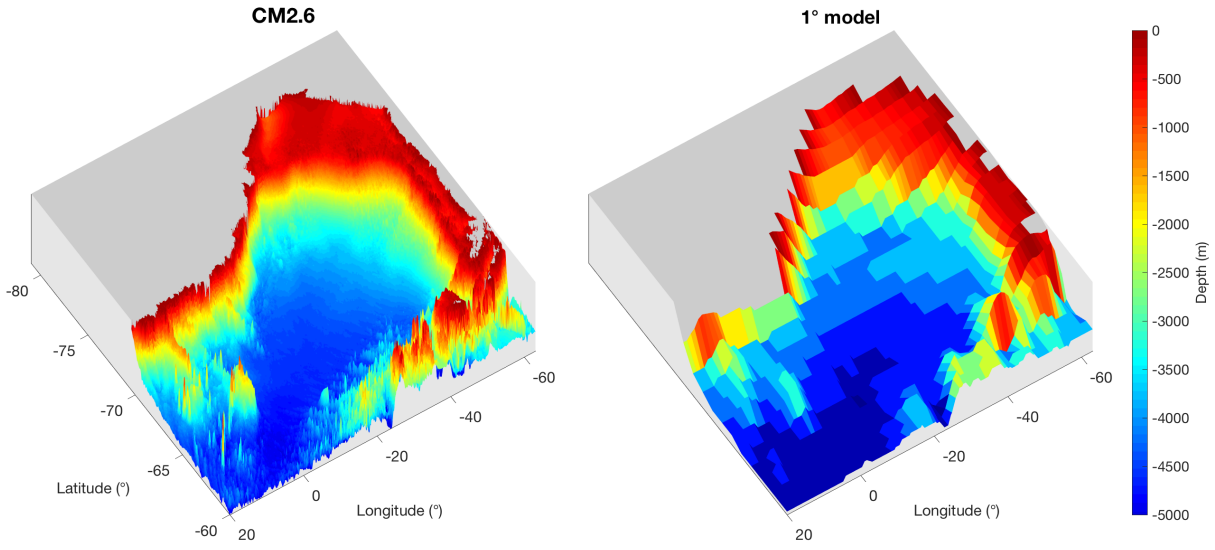

Figure 2–1: Bathymetry of the Weddell Sea for CM2.6 and for a 1° model based on the World Ocean database bathymetry (Conkright et al., 2002).

A reference to "CMIP5 model means" corresponds to all 23 CMIP5 models, unless otherwise stated. Though all analyses were performed on all models, in the following we highlight five CMIP5 models for their representative behavior or peculiarity: ACCESS1-0, GFDL-CM3, HadGEM2-ES, IPSL-CM5A-LR and MPI-ESM-MR. The multi-model mean transient climate response for the full suite of Atmosphere-Ocean General Circulation CMIP5 models is 1.8° K over the 1pctCO_2 experiment (Flato et al. 2013). CMIP5 models are therefore generally less sensitive to the 1pctCO_2 experiment compared to CM2.6.

2.1.3 LLC_4320 model

LLC_4320 is an ocean/sea-ice model based on the MIT general circulation model (MITgcm; Rocha et al. 2016), configured with the very fine horizontal grid spacing of 1/48°. It also has 90 depth levels, ranging from 1 m at the surface to 480 m at a depth of 7000 m. The 16 most dominant astronomical tidal forcing components are included to allow for the representation of realistic tides. In addition, the simulation is forced by 6-hourly 0.14° European Centre for Medium-Range Weather Forecasts analysis (ECMWF, 2011).

With its very fine grid spacing, the LLC_4320 simulation resolves mesoscale eddies on the continental shelves of Antarctica and is the first ocean-sea ice model capable of resolving circum-Antarctic mean flows, eddies and tides together (Stewart et al., 2018). Analyses of the LLC_4320 simulation have shown good congruence to observations (Stewart et al., 2018). Hence, we evaluate the ASF and ASC in CM2.6 and CMIP5 with that in LLC_4320 (Section 3.34.1).

The LLC_4320 output we use is described in Stewart et al. (2018) and spans September 2011 to October 2012, where 6-hour snapshots are averaged over the full time period. The model output was retrieved from a publicly available repository (http://metadata.imas.utas.edu.au/geonetwork/srv/eng/metadata.show?uuid=99ccd395-af52-4a36-bca4-edd7991435bd).

2.1.4 Simulations

We use two experiments; a piControl and a 1pctCO_2 simulation (Fig. 2–2). The piControl for CM2.6 is run for 200 years under 1860 preindustrial atmospheric forcing based on a constant globally averaged CO_2 mixing ratio of 286 ppm by volume (ppmv). The climate change simulation is an idealized +1% yr^{-1} CO_2 (1pctCO_2) rise experiment branched off from the piControl at year

Model	Ocean resolution	Atmosphere resolution	Gravitational instability
CM2.6	0.1°	0.45 °	enhanced vertical diffusivity & viscosity
ACCESS1.0	1°	1.25° × 1.875°	enhanced vertical diffusion
ACCESS1.3	1°	1.25° × 1.875°	enhanced vertical diffusion
BCC-CSM1.1	0.33° - 1°	2.7° × 2.8°	enhanced vertical diffusion
BCC-CSM1.1m	0.33° - 1°	2.7° × 2.8°	enhanced vertical diffusion
CNRM-CM5	1° × 0.65°	1.4 °	enhanced vertical diffusion
CNRM-CM5-2	1° × 0.65°	1.4°	enhanced vertical diffusion
CSIRO-Mk3.6.0	1.8° × 0.93°	1.8°	convective adjustment
CSIRO-Mk3L-1-2	2.8° × 1.6°	3.2° × 5.6°	enhanced vertical diffusion
FGOALS-g2	0.5° - 1°	2.8°	convective adjustment
FGOALS-s2	0.5° - 1°	1.6° × 2.8°	convective adjustment
GFDL-CM3	0.33° - 1°	2° × 2.5°	enhanced vertical diffusion
GFDL-ESM2G	0.33° - 1°	2 °	included turbulence closure
GFDL-ESM2M	0.33° - 1°	2° × 2.5°	enhanced vertical diffusion
HadGEM2-ES	0.33° - 1°	1.25° × 1.8°	enhanced vertical diffusion
INMCM4	0.5° - 1°	1.5° × 2°	enhanced vertical diffusion
IPSL-CM5A-LR	1.9° × 1.3°	1.8° × 3.75°	enhanced vertical diffusion
IPSL-CM5A-MR	1.9° × 1.3°	1.2° × 2.5°	enhanced vertical diffusion
IPSL-CM5B-LR	1.9° × 1.3°	1.8° × 3.75°	enhanced vertical diffusion
MIROC5	0.5° × 1.4°	1.4°	convective adjustment
MPI-ESM-LR	1.5°	1.8°	enhanced vertical diffusion
MPI-ESM-MR	0.4°	1.8°	enhanced vertical diffusion
MPI-ESM-P	1.4 ° × 1°	1.8°	enhanced vertical diffusion
MRI-CGCM3	0.5° × 1°	1°	convective adjustment

Table 2–1: Model comparison of ocean and atmospheric horizontal resolutions, and treatment of gravitational instability in the ocean.

121. Doubling of atmospheric CO_2 concentration occurs after 70 years of the simulation after which the concentration is held at 572 ppm for ten years.

The piControl experiment for CMIP5 is set to atmospheric concentrations of 286.15 ppmv, 790.9 ppbv and 275.4 ppbv for CO_2, CH_4 and N_2O, respectively (Taylor et al., 2012). The same 1pctCO_2 simulation described for CM2.6 is used for all CMIP5 models. For the entire duration of the experiment, all non-CO_2 forcing agents (CH_4, N_2O, tropospheric and stratospheric O_3, tropospheric sulfates, black and organic carbon, dust, sea salt, and solar irradiance) are held constant at values representative of year 1860. Only a single run ('r1i1p1') is used for each CMIP5 model. Note that we use the piControl and 1pctCO_2 simulations, instead of the historical and

Representative Concentration Pathway 8.5 (RCP8.5) simulations that are discussed in de Lavergne et al. (2014), to allow for a more direct comparison of the CMIP5 models with CM2.6 for which no historical nor RCP8.5 simulation are available.

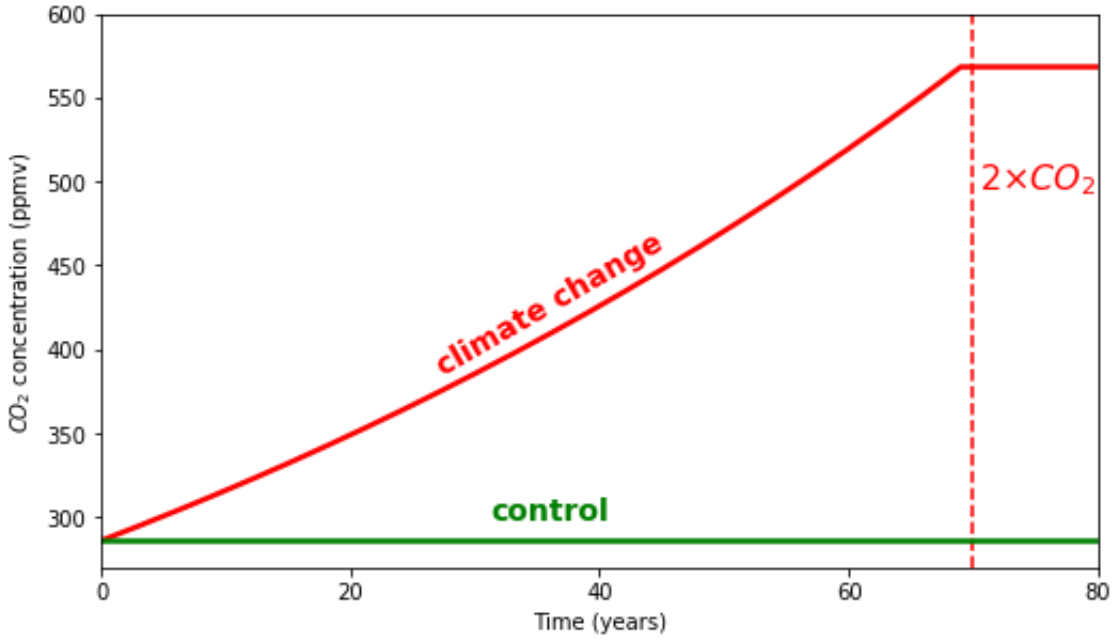

Figure 2–2: CO_2 concentrations for the piControl (green) and 1pctCO_2 (red) model simulation.

2.2 Observations

Observational profiles of temperature and salinity used in this study are from the World Ocean Database (WOD), spanning from 1920 to 2018 in the open ocean Weddell Sea (Fig. 2–3 a; Boyer et al. 2018). This dataset corresponds to 16,071 profiles including observations from regional Argo floats, cruises and instrumented elephant seals. All data is binned into a 0.25° × 0.25° grid. To avoid temporal bias, monthly anomalies are calculated for each year of observations by subtracting the appropriate monthly gridded WOCE/Argo Global Hydrographic Climatology (WAGHC; Gouretski 2018) from the gridded observational profiles. Yearly anomalies are then calculated as the mean of the monthly anomalies for each year. The yearly anomalies for each year are then added to the WAGHC annual climatological mean to produce a yearly temperature and salinity profile for each grid in the depth range from 0 - 2000 m following de Lavergne et al. (2014). We use the winter sea ice extent observations from the Hadley Centre Sea Ice and Sea Surface Temperature data set (HadISST; Rayner et al. 2003) which span from 1970 to 2018;

precipitation (liquid+snow) and evaporation fluxes from the ERA-Interim reanalysis which span from 1979 and 2018 (Dee et al. 2011); and sea ice freezing and melting flux from observational estimates described in Haumann et al. 2016 which are averaged between 1982 and 2008 and which we retrieved from a publicly available repository at https://www.envidat.ch/dataset/10-16904-8.

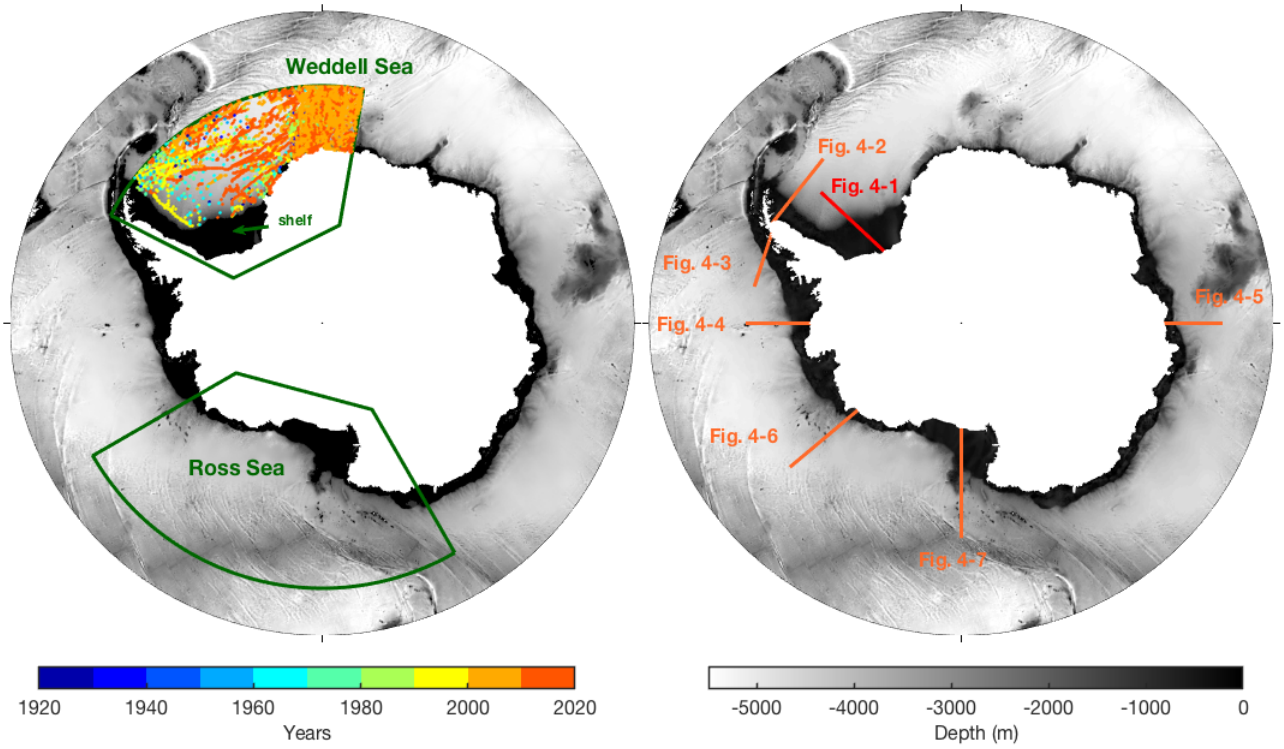

Figure 2–3: Topography (grey shades) of the Southern Ocean (<55° S) depicting the regions of study overlaid with positions and years of observations from the World Ocean Database spanning from 1912 to 2018. Note that the comparison with observations is only performed in the Weddell Sea sector.

2.3 Domain of analysis

The focus of this study is the Southern Ocean (<55° S; Fig. 2–3 a). This region is subdivided into (1) the Weddell Sea, bounded in longitude by the Maud Rise and Antarctic Peninsula (63° W to 10° E) and extending in latitude from the Antarctic Peninsula to the Antarctic continent (63°–78.5° S), and (2) the Ross Sea (60-78.5° S; 140-240° W; Fig. 1 a). The eastern boundary of

the Weddell Sea domain is imposed with the intention of excluding the Maud Rise because this study focuses on fully developed WSPs, not on the episodic small polynyas frequently observed at the Maud Rise (Lindsay et al., 2004). Although often observed prior to full WSPs, Maud Rise Polynyas do not necessarily lead to large polynyas in the Weddell Sea (Comiso and Gordon, 1987; Lindsay et al., 2004). For some models, the intensity of open-ocean deep convection events is sensitive to this spatial limitation, as convection can extend to the East of 10° E and North of 63° S (Section 3.1). However, as the convection is predominately observed in the central Weddell Sea in models, the occurrence of the events is not significantly affected by the choice of the domain. As many models convect in regions outside of the Weddell Sea, we also include the Ross Sea, another privileged region of convection in models, and the full Southern Ocean to allow for investigation of the response of convection to climate change all around Antarctica.

To eliminate coastal polynyas from this study along the same premise as with Maud Rise polynyas and to allow for comparison between the open and shelf regions, the domain of analysis is further divided into the open-ocean region and shelf region using the 1000 m isobath. Due to the effects of rotation and weak stratification of the Southern Ocean, conservation of potential vorticity (PV; Pedlosky 1987; Thompson et al. 2018) constrains the ASC to approximately follow contours of f/h, where f is the Coriolis parameter and h is the depth of the water column. Since f varies negligibly in high latitude regions, the ASC position is tightly constrained by the 1000 m isobath and the 1000 m isobath is thus chosen as an approximation of the position of the ASC (Dufour et al., 2017; Goddard et al., 2017). The locations of the transects used to compare the representation of the ASC and ASF in LCC_4320, CM2.6 and CMIP5 models can be found on Fig. 2–3 b).

In models, convection events are detected by examining the convection area which is defined as the surface area where the September Mixed Layer Depth (MLD) exceeds 2000 m, following de Lavergne et al. (2014). The MLD is determined using a threshold method based on density; $\sigma_\theta(z)$ - $\sigma_\theta(surface)$ = 0.03 kg/m^3, where σ_θ is the potential density referenced to the surface (de Boyer Montégut et al., 2004). Convective models are models containing at least one year in either simulations where the average September convection area exceeds 10^5 km^2 (de Lavergne

Model	Time period
CM2.6	40-57
ACCESS1-0	55-80
ACCESS1-3	48-56
BCC-CSM1.1	58-78
BCC-CSM1-1-m	40-80
CNRM-CM5	40-80
CNRM-CM52	51-80
CSIRO-Mk3L-1-2	58-80
CSIRO-Mk3-6-0	40-80
FGOALS-g2	40-80
FGOALS-s2	40-80
HadGEM2-ES	40-80
GFDL-CM3	40-80
GFDL-ESM2G	71-79
GFDL-ESM2M	66-78
INMCM4	40-80
IPSL-CM5A-LR	67-80
IPSL-CM5A-MR	40-80
IPSL-CM5B-LR	40-80
MPI-ESM-LR	48-80
MPI-ESM-MR	44-66
MPI-ESM-P	69-80
MIROC5	63-80
MRI-CGCM3	40-73

Table 2–2: Time periods for calculation of change under climate change (1pctCO_2 minus piControl) for each model

et al., 2014). For each model, the calculation of change under climate change (1pctCO_2 minus piControl) is carried out over the period corresponding to the longest consecutive non-convective period during the 1pctCO_2 simulation between years 40-80. This choice is made for sake of inter-model comparison as CM2.6 convects towards the end of the 1pctCO_2 simulation, whilst the majority of CMIP5 models have stopped convecting (Section 3.1). Using a fixed time period instead would lead to comparing polynya periods in some models with non-polynya periods in other models. This would be an issue as convection events and associated polynyas significantly impact the surface salinity and freshwater fluxes. The time periods used for each model is available in Table 2–2.

3
Results

3.1 Convection and the WSP in climate models

CM2.6 simulates two Weddell Sea convection events over both the piControl and 1pctCO_2 simulations, each of which result in convection events associated with open ocean polynyas (Fig. 3–1). The relation between convection events and polynya formation in CM2.6 can be deduced from Figure 3–2. Convection events are evident when convective area increases from near zero to above 8×10^5 km^2, with the MLD deepening from an average of approximately 150 m to 1500 m. During each convection event, warm water is transported vertically from depth to the surface resulting in the depletion of the subsurface heat reservoir (SHR). The vertical transport of warm water to the upper ocean melts sea ice, decreasing the normalized winter sea ice concentration from approximately 1 to 0.6, resulting in a polynya. Recharge of the SHR of approximately 1-2 $\times$ 10^8 PJ then occurs, building up to the next convection event. The polynyas observed in CM2.6 are larger and over longer duration compared to the WSP observed in the 1970's (Fig. 3–3).

CMIP5 models show substantial variability with respect to convection and polynya occurrence across the models (Fig. 3–4 and Fig. 3–1). The frequency and duration of convective events in CMIP5 models are highly model dependent with most models showing continuous or quasi-continuous convective activity. The average Weddell Sea winter MLD in CMIP5 models is generally found at depths between 150 m and 200 m, increasing to 1500-2000 m during convection events. Furthermore, convection events in CMIP5 models do not necessarily result in polynyas (Fig. 3–1). This point is most clearly evident in ACCESS1-0, where continuous convection is observed with no change in average winter sea ice concentration associated with a polynya (Fig.3–4 a). As detailed by Dufour et al. (2017), this disconnect between convection and polynyas is also found in the GFDL-CM2.5 climate model, which is configured just as CM2.6 yet with a 0.25° ocean grid spacing rather than the finer 0.10° spacing used in CM2.6.

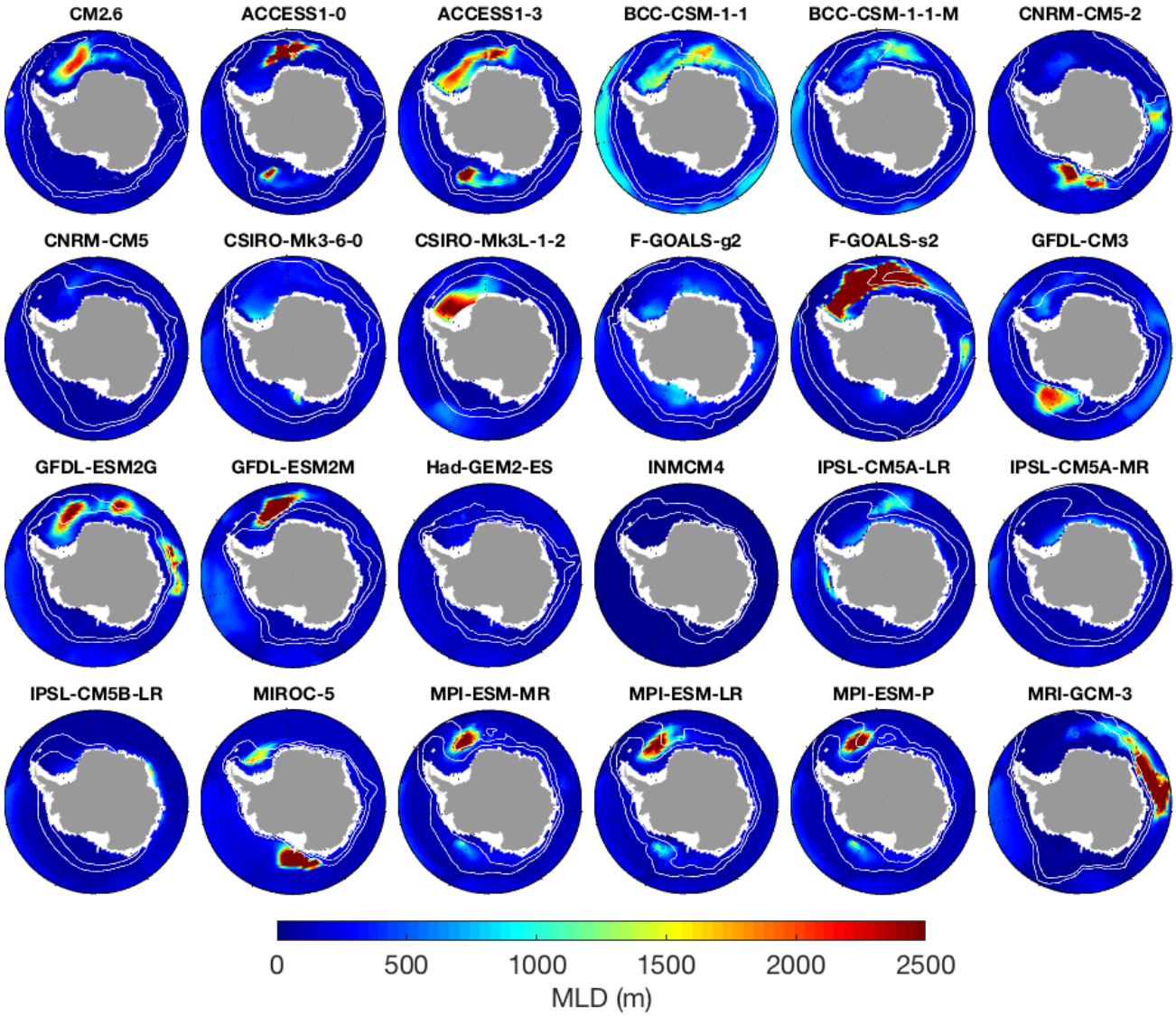

Figure 3–1: Average winter MLD (shading) and sea ice concentrations at 25% & 75% (white contours) over the piControl experiments. Note the masked shelf region shown by white values.

Although convection events in CMIP5 models are predominately found in the Weddell Sea, convective regimes are observed for ten models in the Ross Sea and for four in the Indian Ocean sector of the Antarctic (Fig. 3–5 a-c and Fig. 3–1). Of the 23 CMIP5 models used in this study, four exhibit no convection in all regions. Polynya events in CM2.6 are located only in the Weddell Sea, with no convection events found in the Ross Sea (Fig. 3–5 c). In the Weddell Sea, the majority of CMIP5 models have a mean convection area over the 80 year control of between 1-4 $\times$ 10^5 km^2, whilst CM2.6 exhibits mean convection of 3.27 $\times$ 10^5 km^2 (Table. 3–1).

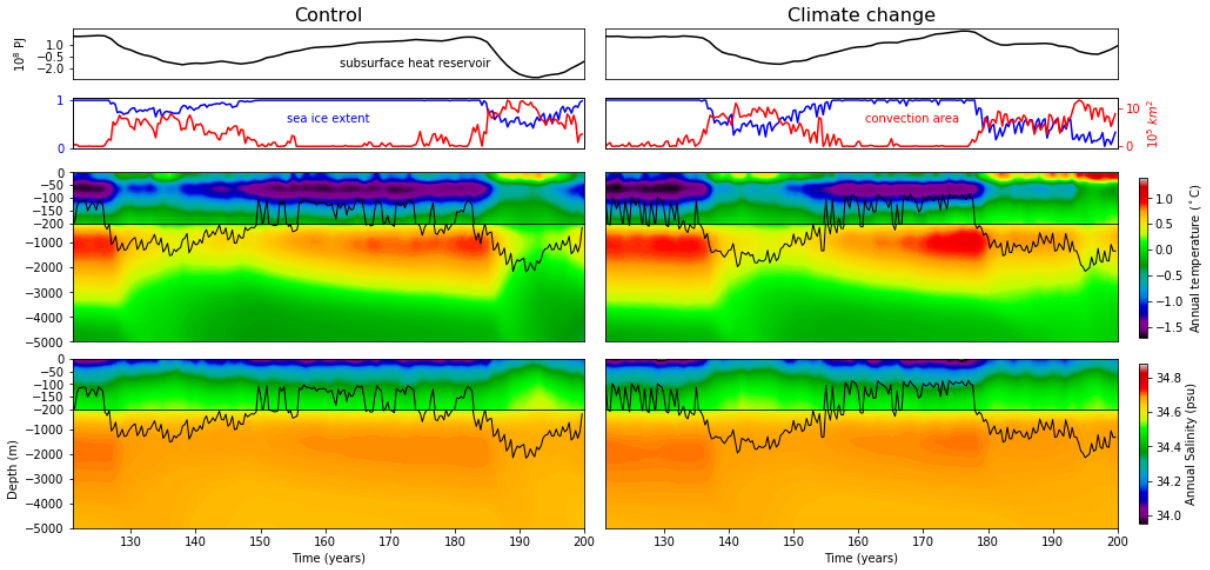

Figure 3–2: Sea ice and thermohaline properties of CM2.6 control (left column) and climate change (right column) simulations averaged over the open ocean Weddell Sea region (See Fig. 2–3). The top panel contains time series of the subsurface heat reservoir (SHR) (gray line; 10^8 PJ). The SHR is defined as the annual heat anomaly, relative to the average heat content over the entire control simulation, building up in the depth range of 200 - 2000 m. The second from top row contains the winter sea ice extent (July-September; blue line) and September convection area (red line). The two lower panels are Hovmöller diagrams (depth vs time) of annual mean potential temperature (°C) and salinity (psu) overlaid with timeseries of winter MLD (black line). Note that there is a zoom on the upper 200 m of the salinity and potential temperature fields. In addition, salinity and potential temperature fields are not fully saturated to allow for visual comparison with Fig.3–4.

Significant discrepancies are visible in thermal structure between models and between models and observations, with models exhibiting both warmer (+0.5° C; Figs. 3–2 and 3–4 b) and cooler (-0.5° C; Fig. 3–4 a,c) temperatures associated with the SHR compared to observations. The modelled SHR in CMIP5 models and CM2.6 extends to approximately 2500 m, whilst in the observations the SHR is shallower, extending to approximately 2000 m (Figs. 3–2 – 3–4). Models with continuous or quasi-continuous convective activity generally simulate low temperatures in the SHR (Fig. 3–4). CM2.6 and most CMIP5 models are in good agreement in range and vertical structure of salinity compared to observations (Figs. 3–2 – 3–4). CM2.6, however, exhibits high salinity below 200 m by approximately 0.1 PSU compared to observations (Figs. 3–2 – 3–3).

Under the 1pctCO_2 simulation, all of the 17 convective CMIP5 models show a decrease in convection area in the Weddell Sea (Figs. 3–4 – 3–5; Table. 3–2) with the multi-model mean

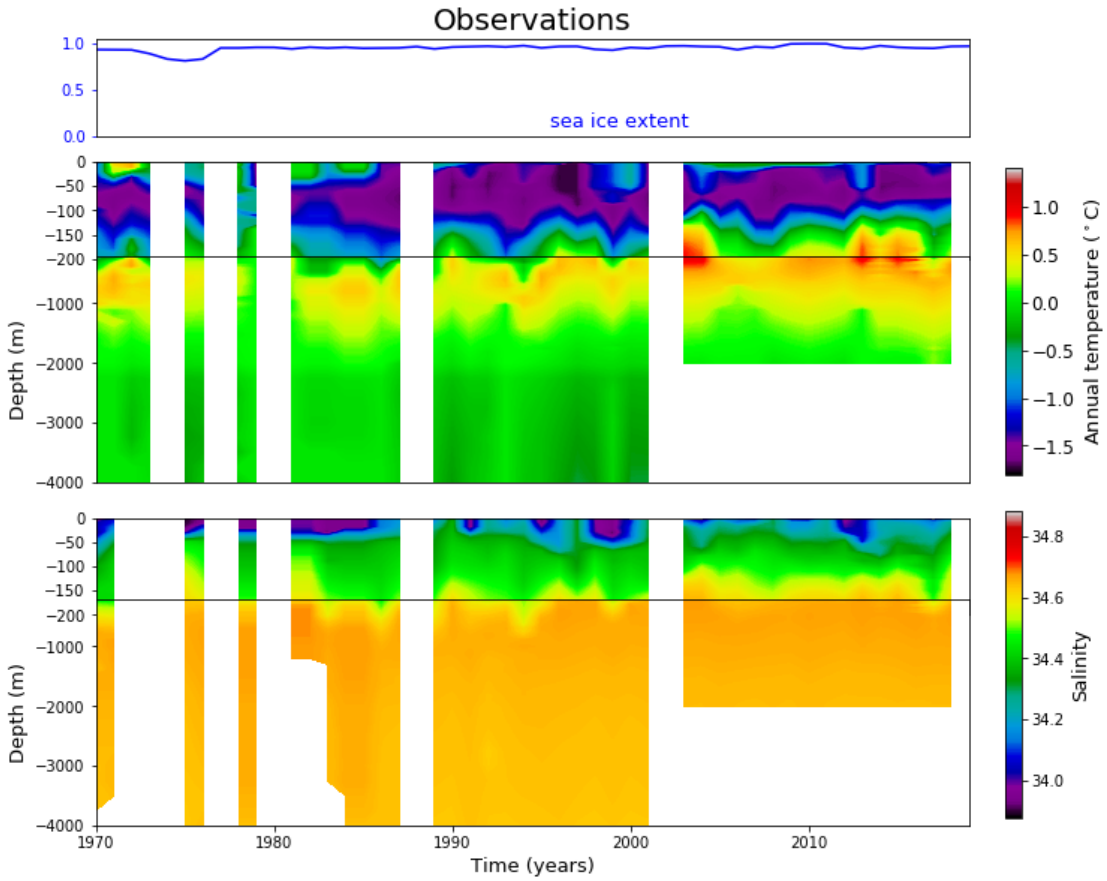

Figure 3–3: Sea ice and thermohaline properties for observations over the open ocean Weddell Sea (see Section 22.2). The top panel contains time series of winter sea ice extent (blue line) from Hadley Centre Sea Ice and Sea Surface Temperature data set (HadISST; Rayner et al. 2003) from 1970 to 2018. Note that the start at 1970 is chosen to show the WSP that occurred in 1974-1976, but does not extend further back as the dataset prior to 1979 is of lower resolution and is less homogeneous (using multiple algorithms) compared to the current satellite period from 1979 onwards. The two lower panels are Hovmöller diagrams (depth vs time) of annual mean potential temperature (°C) and salinity (psu) observations from the WOD spanning from 1970 to 2018 (see Section.2.2). White colors corresponds to missing data.

linear regression trend in convection area of -0.35 $\times$ 10^5 km^2/decade over the sensitivity experiment (Table. 3–2). Out of all convective models, 11 show a full cessation in the Weddell Sea within the 80 years of simulation, whilst seven show a slow down. With this decline in convection intensity under the 1pctCO_2 simulation, there is a corresponding decline in polynya occurrence (see Fig. 3–4 b). The decline in convection area under climate change in CMIP5 models is in good agreement with the results found by de Lavergne et al. (2014), despite using different climate change projections (Section 2.1.4). In stark contrast, the timing, duration and intensity of polynya and convection

Model	Mean convection (10^5 km^2)	Percentage convective years (%)	Upper density stratification (kg/m^3)	Lower density stratification (kg/m^3)
CM2.6	3.27	56.2	0.409	0.345
ACCESS1-0	1.57	76.25	0.526	0.418
ACCESS1-3	3.94	81.3	0.198	0.143
BCC-CSM1.1	1.21	27.5	0.339	0.294
BCC-CSM1-1-m	2.62	53.75	0.299	0.24
CNRM-CM5	0.562	12.5	0.754	0.449
CNRM-CM52	0.543	10.0	0.649	0.359
CSIRO-Mk3L-1-2	7.78	100.0	0.147	0.0891
FGOALS-s2	13.17	100.0	0.185	0.142
GFDL-CM3	1.11	18.75	0.344	0.311
GFDL-ESM2G	4.28	86.25	0.325	0.283
GFDL-ESM2M	3.94	93.75	0.335	0.288
IPSL-CM5A-LR	0.69	13.3	0.352	0.296
MPI-ESM-LR	2.86	87.5	0.378	0.282
MPI-ESM-MR	4.00	97.5	0.399	0.307
MPI-ESM-P	3.43	96.3	0.390	0.297
MIROC5	1.74	51.3	0.216	0.324
MRI-CGCM3	1.42	37.6	1.29	1.01
CSIRO-Mk3-6-0	0.0	0.0	0.264	0.0993
FGOALS-g2	0.0	0.0	0.426	0.121
HadGEM2-ES	0.0369	0.0	0.413	0.311
INMCM4	0.0	0.0	0.967	0.607
IPSL-CM5A-MR	0.0	0.0	0.492	0.431
IPSL-CM5B-LR	0.0	0.0	0.58	0.436

Table 3–1: Averaged convection area, percentage convective years (%) and upper (2000 – 10 m) and lower density stratification (200 – 10 m) for all models averaged over the entire control simulations in the Weddell Sea. The second section of CMIP5 models signifies non-convective models in the Weddell Sea.

events in CM2.6 under the 1pctCO$_2$ simulation are very similar to that of the piControl simulation (Figs. 3–2 and 3–5 a-b).

3.2 Processes controlling convection events

Episodic large deep convection events in the Weddell Sea have been linked in particular to anomalies in the SAM index (Gordon et al. 2007; Cheon et al. 2014; Francis et al. 2019; Campbell et al. 2019; Cheon and Gordon 2019) and in the stratification of the upper ocean (Gordon et al. 2007; Campbell et al. 2019; Cheon and Gordon 2019). Well-known discrepancies in the representation of wind stress strength and position, and of stratification across models, and between

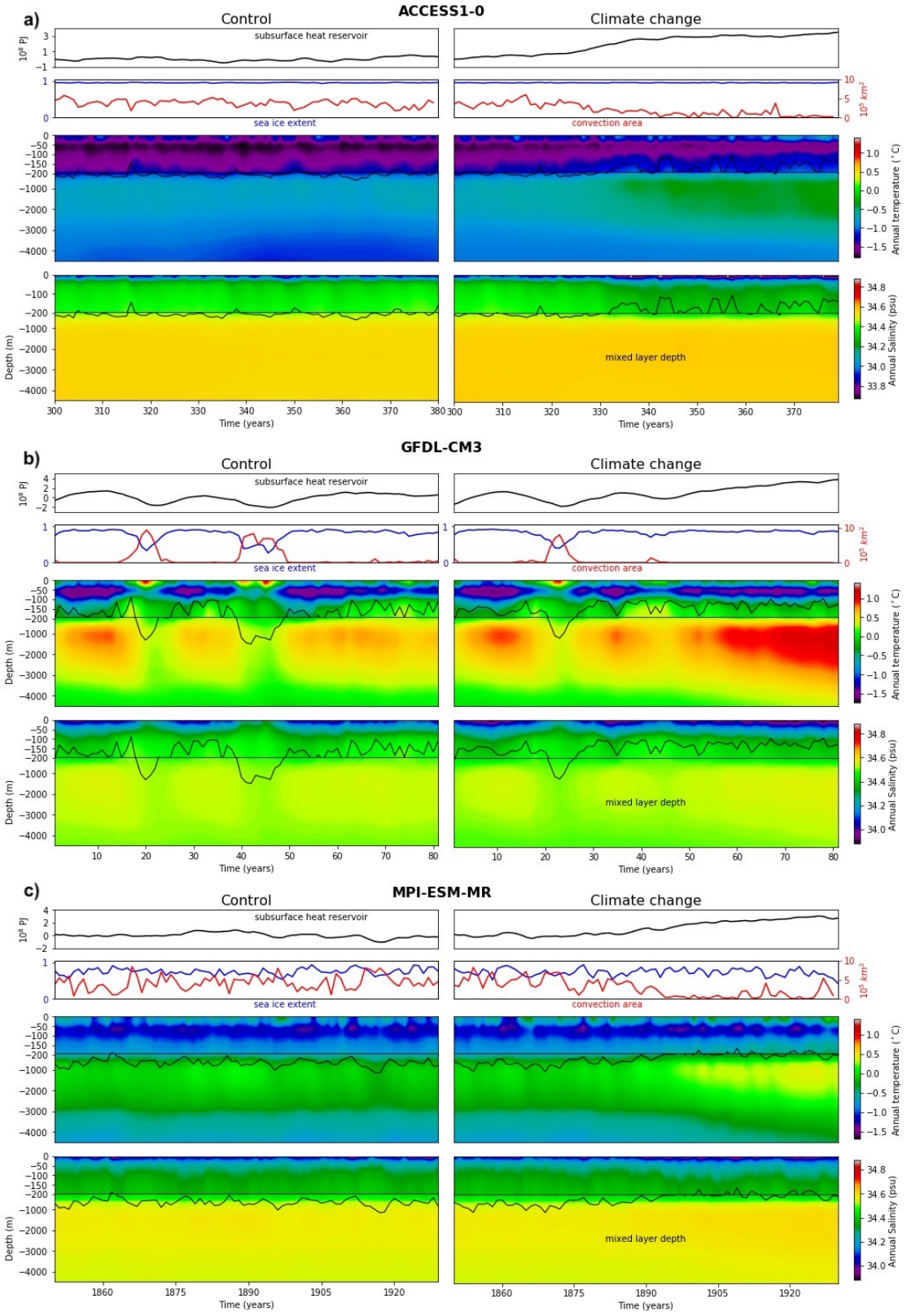

Figure 3–4: Same as Fig. 3–2 but for the a) ACCESS1-0, b) GFDL-CM3 and c) MPI-ESM-MR.

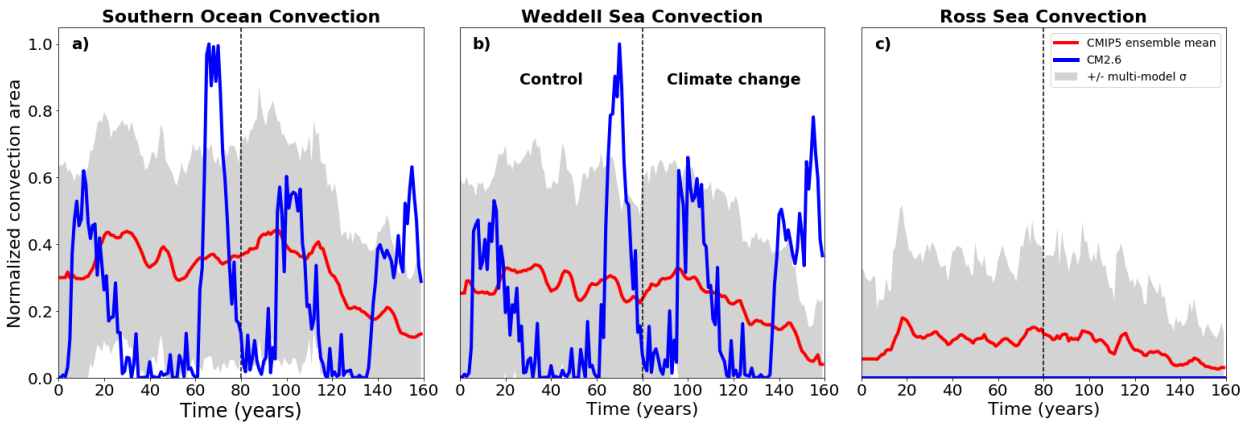

Figure 3–5: Normalized convection area for the CMIP5 model mean (red) and CM2.6 (blue) for the open ocean of a) the Southern Ocean, b) the Weddell Sea and c) the Ross Sea. The grey shading denotes ±1 standard deviation across the CMIP5 models. For each model, the area is normalized by the maximum areal extent of convection recorded over all simulations for that model. The first 80 years denotes the control, with years 80-160 denoting the climate change simulation. The CMIP5 model mean (red line) is computed as a 5 year running mean.

models and observations, make wind and stratification two good candidates to explain the different responses exhibited by CMIP5 models and CM2.6 under the 1pctCO_2 simulation. The position and magnitude of the maximum zonal wind stress over time are very similar between CM2.6 and CMIP5 models under both the control and 1pctCO_2 simulations, with a typical equatorward bias in the maximum westerly position and weak bias in westerly strength evident compared to observations (Fig. 3–6 a,c), as documented in detail in previous studies of CMIP5 models (e.g. Swart and Fyfe, 2012; Bracegirdle et al., 2013). The good congruence in position and strength of SH westerlies between CM2.6 and CMIP5 models allows us to conclude that the response of the SH westerlies to the forcing is likely not the main cause of the continuation of convection in CM2.6 under climate change compared to CMIP5 models. We next explore the role of stratification on convection area.

A relatively weak vertical stratification, which is controlled by salinity from the surface to approximately 2000 m, regulates convection and polynya occurrence in the Weddell Sea in both observations (Campbell et al., 2019; Cheon and Gordon, 2019) and climate models (Martin et al., 2013; de Lavergne et al., 2014; Stössel et al., 2015; Dufour et al., 2017). Over the control simulation, the majority of models show good agreement in vertical potential density difference (density at 2000 m minus at 10 m) and surface salinity as compared to observations (Fig. 3–7). The majority

of convective models have average control vertical potential density difference between 0.3 and 0.4 kg m^{-3} and average surface salinity between 34.0 and 34.3 PSU, whilst observations exhibit an average potential density difference and surface salinity of 0.46 kg m^{-3} and of 34.3 PSU, respectively (Fig. 3–7). In the control simulation, models with large average convective activity in the Weddell Sea have weaker density stratification and higher surface salinity (0 - 100 m) compared to models with low average convection area.

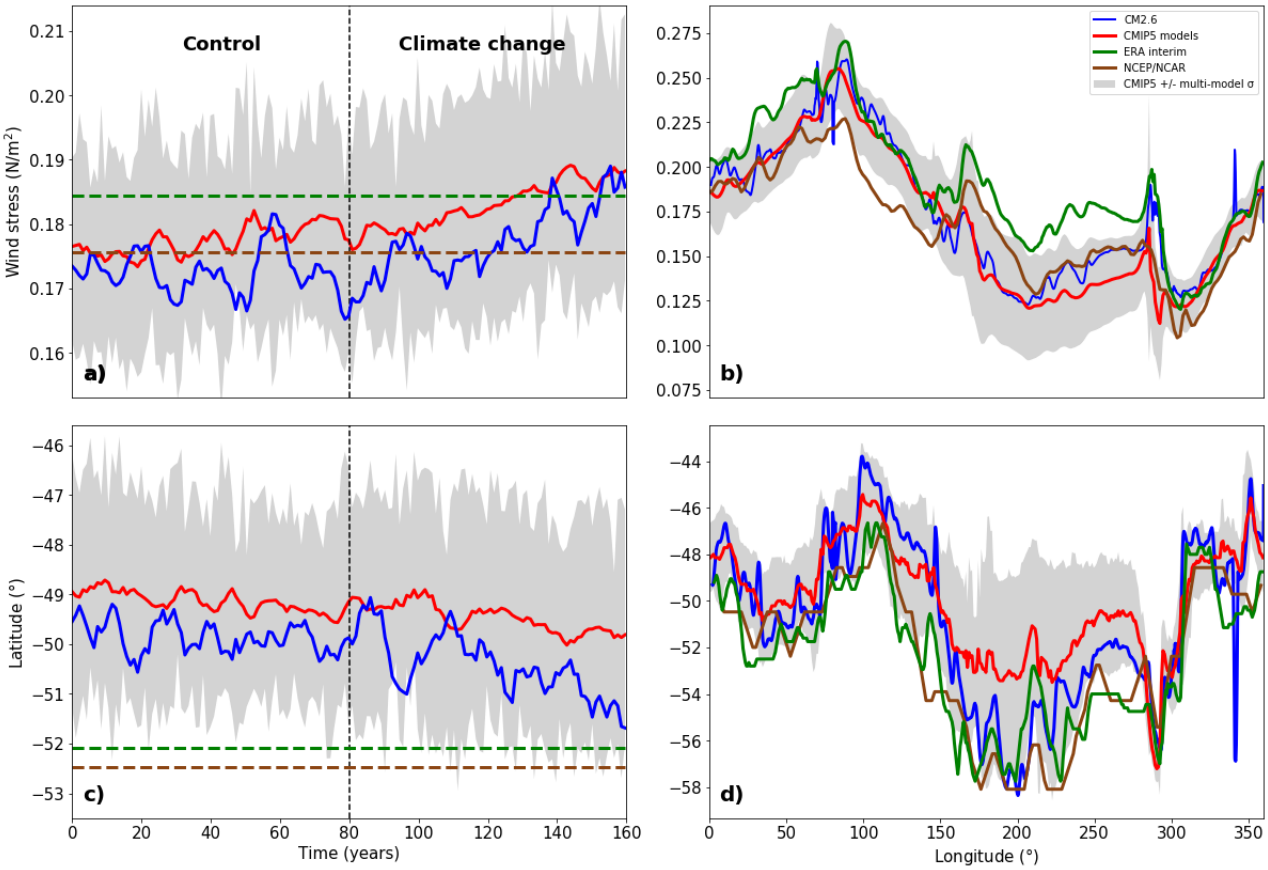

Figure 3–6: a) Magnitude and c) position of maximum zonal mean wind stress over the ocean with time and b) strength and d) latitudinal position of maximum wind stress with longitude over the ocean South of 40S. Models are compared to ERA-Interim reanalysis averaged over years 1979-2019 (https://www.ecmwf.int/en/research/climate-reanalysis/era-interim) and to NCEP/NCAR reanalysis averaged over years 1948-2019 (https://www.esrl.noaa.gov/psd/data/gridded/data.ncep.reanalysis.html). A 5 year moving mean is applied to both reanalysis and model data. The list of models used for the calculation of the CMIP5 model mean is presented in Table. 3–3. Horizontal dashed lines in the left column are averages for ERA-Interim (green) and NCEP/NCAR reanalyses (brown) over the full time periods.

For 16 of the 17 convective CMIP5 models in the Weddell Sea, the slowing of convection activity in the 1pctCO_2 simulation coincides with surface freshening and an increase in vertical

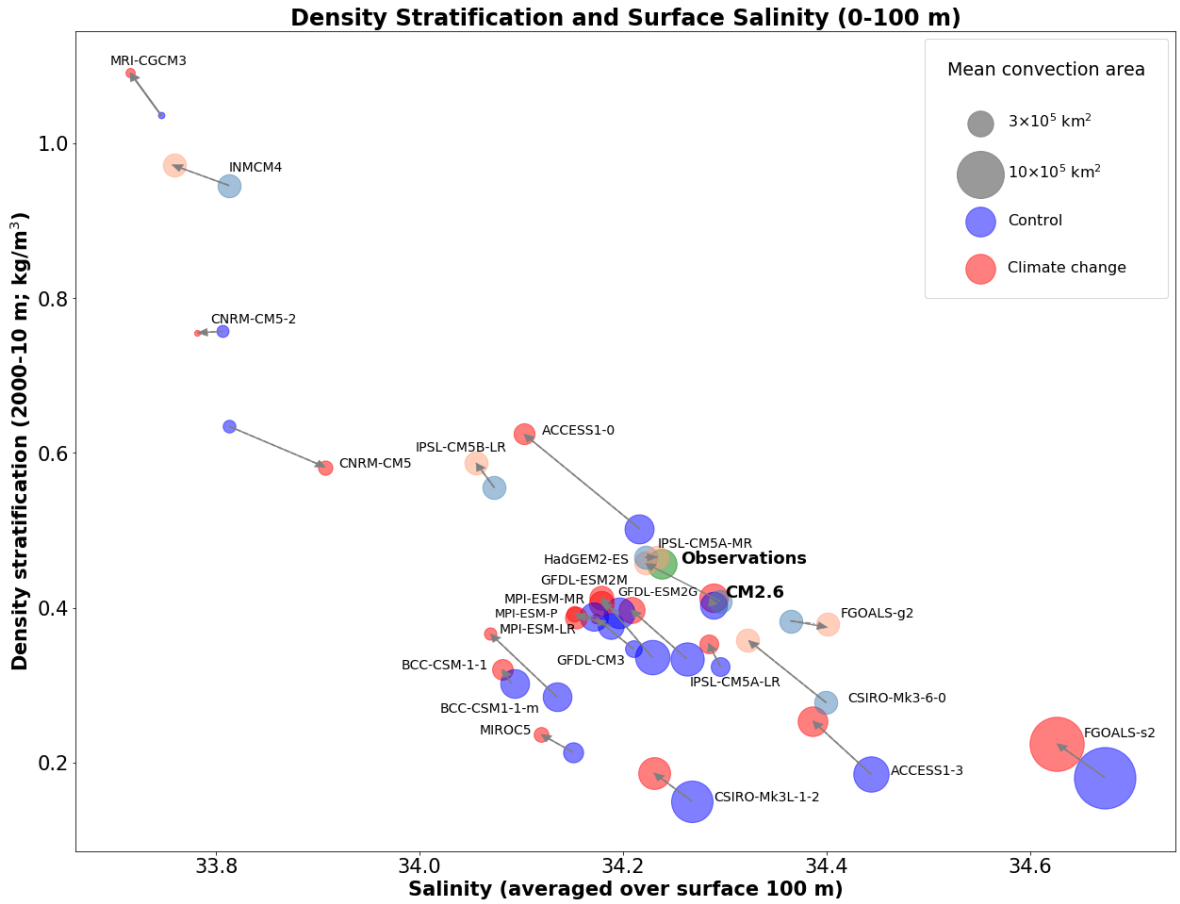

Figure 3–7: Convection area over the control (blue) and climate change (red) simulations in the open ocean Weddell Sea as a function of average surface salinity over the top 100 m and density stratification (2000 - 10 m density difference). Pale coloured models correspond to non-convective models in the Weddell Sea, defined as models that do not have a year where the September convection area exceeds 10^5 km^2. Averages are over the full 80 years of each simulation as not all models convect during the same periods. Observations (green) are plotted with the average convection area of the 1970's WSP and average salinity and density stratification for the WOD profiles spanning from 1920 to 2018. Most CMIP5 models undergo an increase in stratification in response to the 1pctCO_2 forcing (visible by the arrow pointing up), concurrent with a decrease in surface salinity (arrows pointing to the left) and decrease in convection are (larger blue than red circles).

density gradient (Fig. 3–7). CMIP5 models exhibit a multi-model mean linear regression in open ocean surface salinity of -0.0012 PSU/decade and in vertical potential density difference of 0.0059 kg/m^3/decade over the sensitivity experiment in the Weddell Sea (Table. 3–2). CNRM-CM5 is the only convective model that shows a decrease in density stratification and increase in surface salinity in response to the 1pctCO_2 simulation in addition to a decrease in convection area (Fig. 3–7). While the cause of CNRM-CM5 response to the 1pctCO_2 forcing is unclear, we note that

this model is unique within the CMIP5 model group investigated in that it has a very strong Weddell Deep Water temperature bias of approximately +1° C compared to the group average. All convective models, expect CNRM-CM5, exhibit strong and significant positive correlations (r = 0.45 to 0.89) between surface salinity and convection area under the sensitivity experiment (Table. 3–2).

Model	Convection area ($10^5 \times km^2$/decade)	Surface salinity (PSU/decade)	Density stratification (kg/m^3/decade)	Correlation convection area and salinity
CM2.6	0.314	0.0009	0.00045	**0.49**
ACCESS1-0	**-0.53**	**-0.025**	**0.013**	**0.80**
ACCESS1-3	**-0.35**	**-0.018**	**0.012**	**0.58**
BCC-CSM1.1	**-0.42**	**-0.009**	**0.0058**	**0.81**
BCC-CSM1-1-m	**-0.37**	**-0.03**	**0.019**	**0.69**
CNRM-CM5	-0.023	0.0076	**-0.0079**	-0.23
CNRM-CM52	-0.146	**-0.0287**	**0.015**	**0.48**
CSIRO-Mk3L-1-2	**-0.62**	**-0.015**	**0.91**	**0.78**
FGOALS-s2	**-1.264**	**-0.015**	**0.0054**	**0.89**
GFDL-CM3	**-0.14**	**-0.0090**	**0.0103**	**0.58**
GFDL-ESM2G	**-0.33**	**-0.022**	**0.017**	**0.68**
GFDL-ESM2M	**-0.23**	**-0.0086**	**0.0034**	**0.67**
IPSL-CM5A-LR	**-0.066**	**-0.0016**	**0.0052**	**0.84**
MPI-ESM-LR	**-0.35**	**-0.0075**	**0.00089**	**0.57**
MPI-ESM-MR	**-0.68**	**-0.0089**	**0.00427**	**0.77**
MPI-ESM-P	**-0.38**	**-0.0079**	0.00135	**0.63**
MIROC5	**-0.025**	**-0.0058**	0.0015	**0.62**
MRI-CGCM3	**-0.013**	**-0.0091**	**0.0061**	**0.45**
CSIRO-Mk3-6-0	0.0	**-0.023**	**0.0069**	0
FGOALS-g2	0.0	**0.0057**	-0.00125	0.0
HadGEM2-ES	-0.0081	**-0.034**	**0.0060**	0.23
INMCM4	0.0	**0.011**	**0.0099**	0.0
IPSL-CM5A-MR	0.0	0.0017	0.0035	0.0
IPSL-CM5B-LR	0.0	**-0.0090**	0.0015	0.0

Table 3–2: Linear regression per decade over the full 1pctCO$_2$ experiment in convection area, surface salinity and upper density stratification. The second group of CMIP5 models corresponds to the non-convective models in the Weddell Sea. The last column is the r value correlation between salinity and convection area. Bold values indicate significant trends to 95%.

In contrast to the CMIP5 models, the piControl versus the 1pctCO$_2$ simulations for CM2.6 do not show a significant difference in the open ocean surface salinity nor in the vertical potential density gradient (Table. 3–2). CM2.6 simulates a very small increase in open ocean potential density stratification, surface salinity and convection area within the Weddell Sea by the end of

the simulation (Fig. 3–7). The change under climate change in surface salinity (0.007 PSU) and convection area (0.41×10^5 km^2) over the 1pctCO$_2$ simulation is within one standard deviation of control simulation surface salinity (0.06 PSU) and convection area (3.68×10^5 km^2) in the Weddell Sea, and as such, cannot be distinguished from the model's natural variability.

In summary, when subject to the 1pctCO$_2$ forcing, CM2.6 responds with a statistically insignificant increase in convection area, density stratification and surface salinity. CMIP5 models, in contrast, show a statistically significant slowdown, or even cessation, of convection events in the 1pctCO$_2$ simulation that is most likely due to a surface freshening over the convective regions and associated increased stratification.

3.3 Freshening under climate change

3.3.1 Surface water fluxes and freshening

In the CMIP5 and CM2.6 models, the water flux into the ocean (WFO) is the sum of precipitation, evaporation, sea ice (melting and freezing) and runoff (river runoff and iceberg calving). Time mean precipitation and evaporation intensify with decreasing latitude, reaching a maximum at approximately 45°S (Fig. 3–8 a,c). In all models, the zonally averaged precipitation and evaporation fluxes are generally in good agreement with ECMWF-Interim reanalysis (ERA-Interim; Dee et al. 2011) but show a high bias in precipitation and in evaporation (Fig. 3–8 a,c). Sea ice fluxes exhibit large negative zonal values at high latitudes ($\leq$ 75°S) due to sea ice formation in the vicinity of the continent with modelled sea ice freezing overestimated as compared to observational estimates (Haumann et al. 2016; Fig. 3–8 e). Runoff near the continent in CM2.6 is higher compared to most CMIP5 models (Fig. 3–8 g), and in combination with more freezing/formation of sea ice, results in CM2.6 having a lower mean state WFO at higher latitudes (Fig. 3–8 i). Between 60°S and 80°S, CNRM-CM5 and IPSL-CM5A-MR exhbit negative integrated WFO changes (Table. 3–4). Omitting these models results in CMIP5, we find that the WFO change in the open ocean and shelf are of 0.0056 Sv and 0.0038 Sv (Sv = 10^9 kg s^{-1}) respectively. In CM2.6, WFO changes on the shelf and open ocean are of 0.0087 Sv and 0.0032 Sv respectively. Hence, the open ocean WFO change in CM2.6 is within one standard deviation of that of the CMIP5 model ensemble, implying that CM2.6 does not show particularly weak flux of water into the open ocean in

comparison to CMIP5 models that could have explained the continued convection in that model. On the shelf, the WFO change in CM2.6 is larger than one standard deviation of the CMIP5 model ensemble (Table. 3–4). We note that in all models, the integrated WFO are largest within the shelf region.

CMIP5 models and CM2.6 demonstrate an increase in WFO under climate change, predominately between 60°S and 80°S (Fig. 3–8 j). Decomposition of the surface fluxes reveals that the change in WFO can be attributed predominately to sea ice flux change and to enhanced runoff (Fig. 3–8 f,h), resulting in higher input of freshwater into the upper ocean under climate change. Thus, the increased WFO explains the lower surface salinity under climate change as seen in Section 3.2. This increase in WFO is larger in CM2.6 than in most CMIP5 models, hence ruling out a lack of freshening in CM2.6 to explain the absence of a change in open Weddell Sea salinity under climate change.

Variable	Models
Surface downward x stress (tauvo)	ACESS1.0, ACESS1.3, BCC-CSM1.1m GFDL-CM3, CNRM-CM5, CNRM-CM5-2 CSIRO-MK3.6, CSIRO-Mk3l-1-2, FGOALS-s2 GFDL-CM3, GFDL-ESM2G, GFDL-ESM2M IPSL-CM5A-LR, IPSL-CM5A-MR, IPSL-CM5B-MR INM-CM4, MIROC5, MPI-ESM-LR MPI-ESM-MR, MPI-ESM-P
Runoff (ficeberg & friver)	GFDL-CM3, GFDL-ESM2M GFDL-CM3
Sea ice flux (fsitherm)	ACCESS1-0, ACCESS1-3 GFDL-ESM2M, GFDL-CM3 HadGEM2-ES,IPSL-CM5A-LR IPSL-CM5A-LR, IPSL-CM5A-MR MIROC5
WFO (wfo)	ACCESS1-0, ACCESS1-3 CNRM-CM5, CNRM-CM5-2 GFDL-ESM2G, GFDL-CM3 GFDL-ESM2M, HadGEM2-ES IPSL-CM5A-LR, IPSL-CM5A-MR MIROC5, MPI-ESM-LR MPI-ESM-MR

Table 3–3: The models used to create the CMIP5 model means for Fig. 3–6 and 3–8.

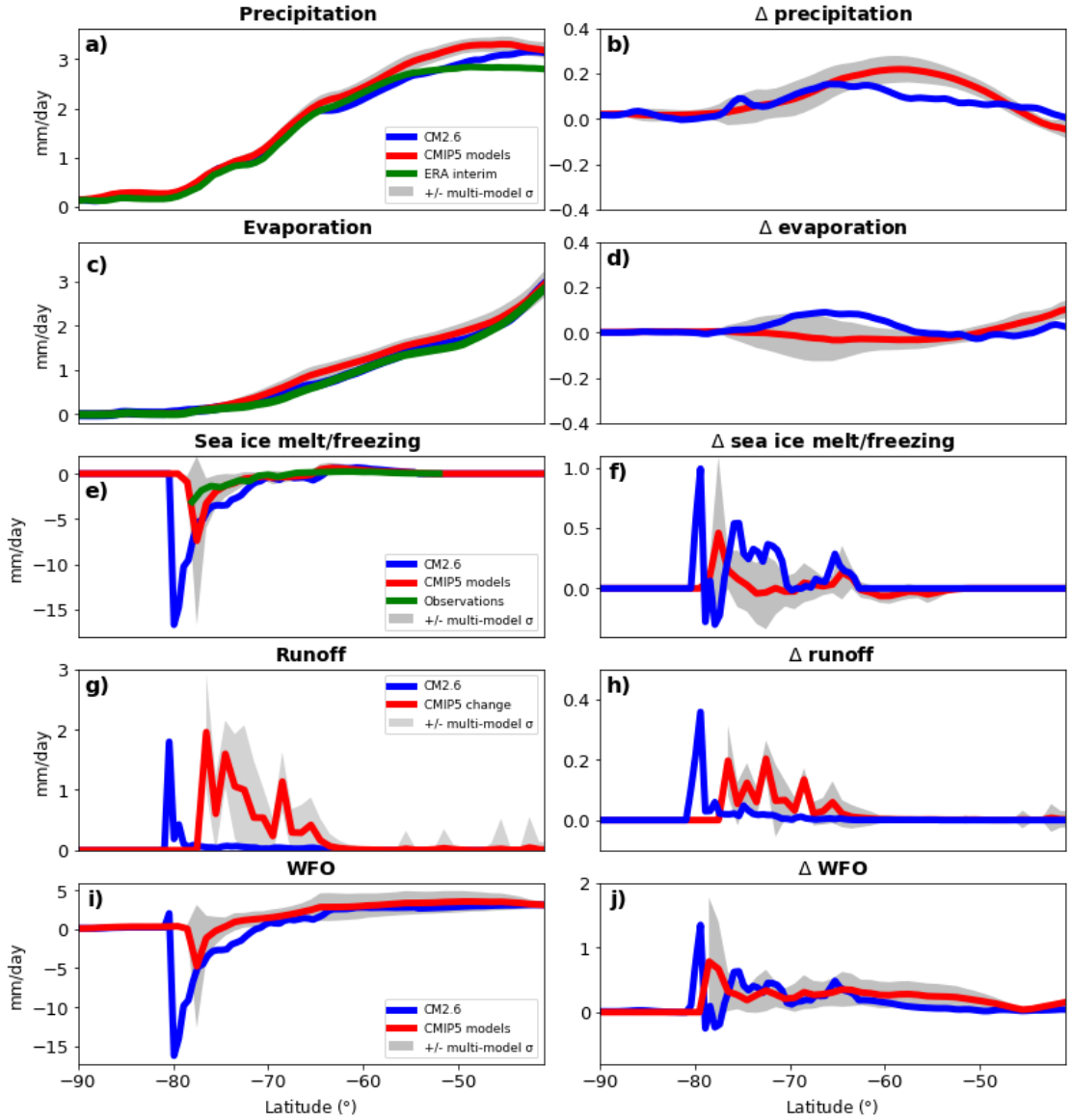

Figure 3–8: (left) Zonally averaged surface flux in the control simulations for CM2.6 and CMIP5 models. (a) Precipitation (liquid+snow) and (c) evaporation averaged between 1979 and 2018 in ERA-Interim reanalysis (green line; Dee et al. 2011). (e) Sea ice freezing and melting flux averaged between 1982 and 2008 from observational estimates described in Haumann et al. 2016 and retrieved from a publicly available repository at https://www.envidat.ch/dataset/10-16904-8 (green line). (Right) Zonally averaged change in flux rate under climate change. (i) Water Flux into the Ocean (WFO) corresponds to the sum of precipitation, evaporation, sea ice melt and freezing, and runoff fluxes. Runoff refers to the combined river runoff and iceberg calving flux into the ocean. (j) Response of WFO to climate change. Positive values denote a positive flux into the surface ocean. Because not all variables were available for the 23 CMIP5 models used in this study, the models used to compute the CMIP5 models means and standard deviations (red and shaded colors) for each panel are listed in Table. 3–3. CMIP5 model precipitation and evaporation fluxes (a-d) are for all 23 CMIP5 models used in this study.

In response to CO_2 forcing, both the Weddell Sea shelf and open ocean regions significantly freshen in 20 of the CMIP5 models (Fig. 3–9 and 3–10) with different magnitude across models. CM2.6 exhibits one of the largest depth averaged freshening in the Weddell Sea shelf region of all CMIP5 models (Fig. 3–10) but near zero salinity change in the open ocean (Fig. 3–10), meaning that the freshening is predominately confined to the shelf region in this model. This geographical confinement of the freshening anomaly points to the existence of a dynamical barrier that prevents freshening from spreading offshore. Considering the regional ocean dynamics and circulation, this barrier could be provided by the ASC and ASF (Jacobs, 1991; Thompson et al., 2018).

3.3.2 Control of the freshwater anomalies by the ASC and ASF

CM2.6 exhibits a strong westward ASC, consisting of numerous zonal jets with time average velocities exceeding 0.2 m s^{-1} in the Weddell Sea (Fig. 3–11). While the ASC is present all around Antarctica in CM2.6, it is generally weak or absent along the West Antarctic Peninsula and in the Bellinghausen Sea (Fig. 3–11). A combination of wind forcing, advection, mixing and bathymetry of the Antarctic margins force and modulate the ASC (Thompson et al., 2018).

Observed gradients in water mass properties are very strong across the ASC, between the cool and fresh shelf waters and the warmer and saline open ocean Circumpolar Deep Water, with this gradient forming the ASF (Whitworth et al., 2013). In CM2.6, the ASC is accompanied by a strong ASF, as evident by the prominent cross-shelf density, temperature, salinity and sea level gradients (Fig. 3–12 a-d). Additionally, the ASF manifests through strong isopycnal doming towards the continental shelf in CM2.6 (Fig. 3–13). The lateral density gradients across the ASF contribute to establishing the geostrophically balanced, vertically sheared along-slope flows of the ASC, such that the density field influences the vertical structure of the ASC (Thompson et al., 2018). In CM2.6, the dynamics associated with the ASF and ASC constrains the coastal freshening to remain close to the coast (Fig. 3–13).

In the coarser resolution CMIP5 models, current speeds in proximity to the Antarctic continent rarely exceed 0.05 m s^{-1} (Fig 3–11). Most CMIP5 models do not explicitly resolve continental shelf bathymetry and as a result are largely unable to simulate the ASC, represent topographic steering of the ASC nor capture the lateral gradients in salinity or density associated with the

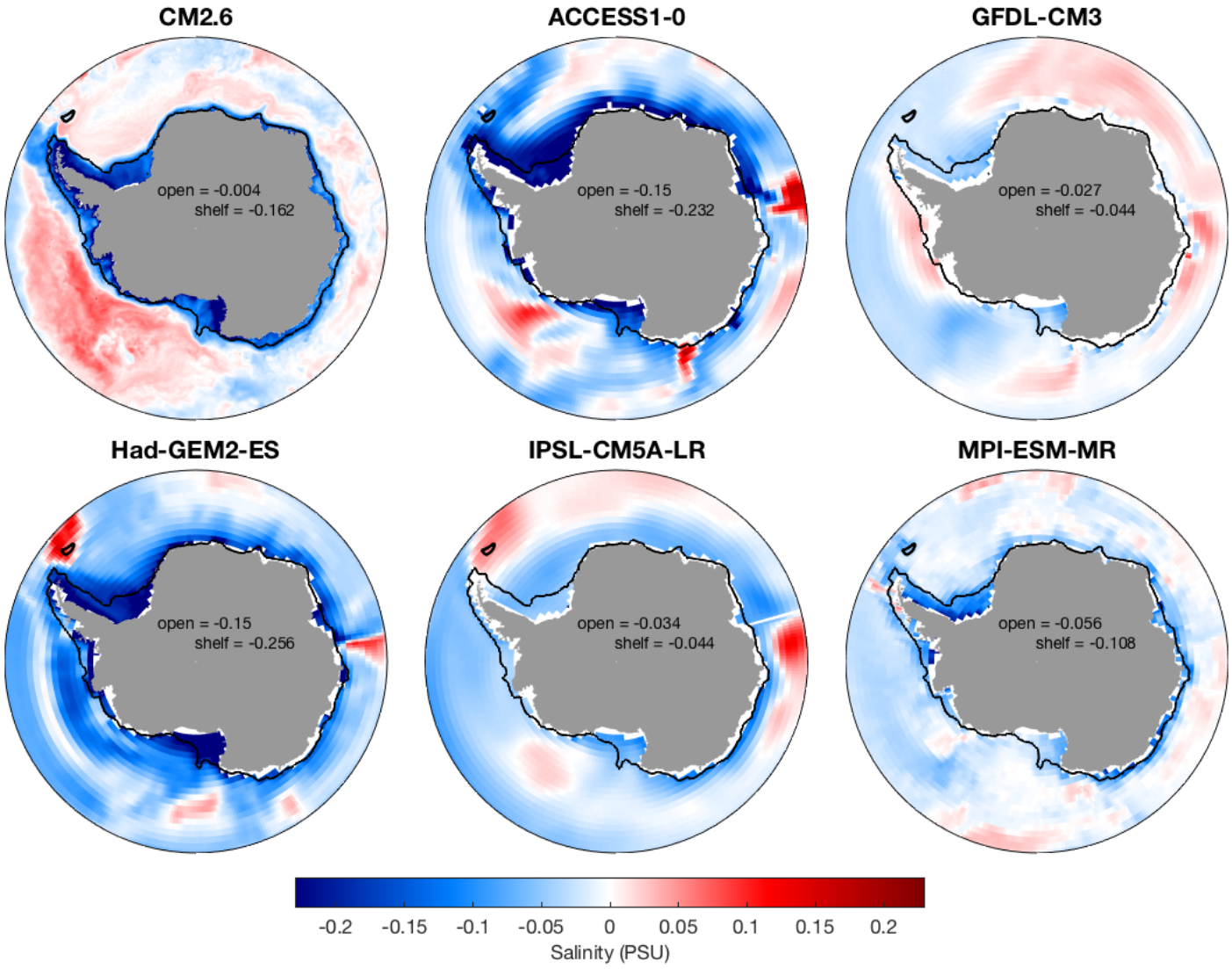

Figure 3–9: Depth average salinity change (0-1000 m; 1pctCO_2 minus piControl) with the 1000 m isobath (black contour) for the full Southern Ocean region. The lower bold values on the continent are the depth averaged (0 - 1000) salinity change for the shelf region in the Weddell Sea (defined using the 1000 m isobath) whilst the upper values refer to the open ocean salinity change in the Weddell Sea.

ASF (Fig. 3–13). In CMIP5 models with finer horizontal ocean resolution, we find higher speed and larger meanders in the ASC, most notably in the Weddell Sea (Fig. 3–11). In particular, MPI-ESM-MR, which has a horizontal ocean grid spacing of 0.4° ×0.4°, has a more coherent ASC with higher depth averaged speed than the coarser resolution CMIP5 models (Fig. 3–11) in addition to displaying a weak ASF (Fig. 3–13). The poor representation of the shelf versus

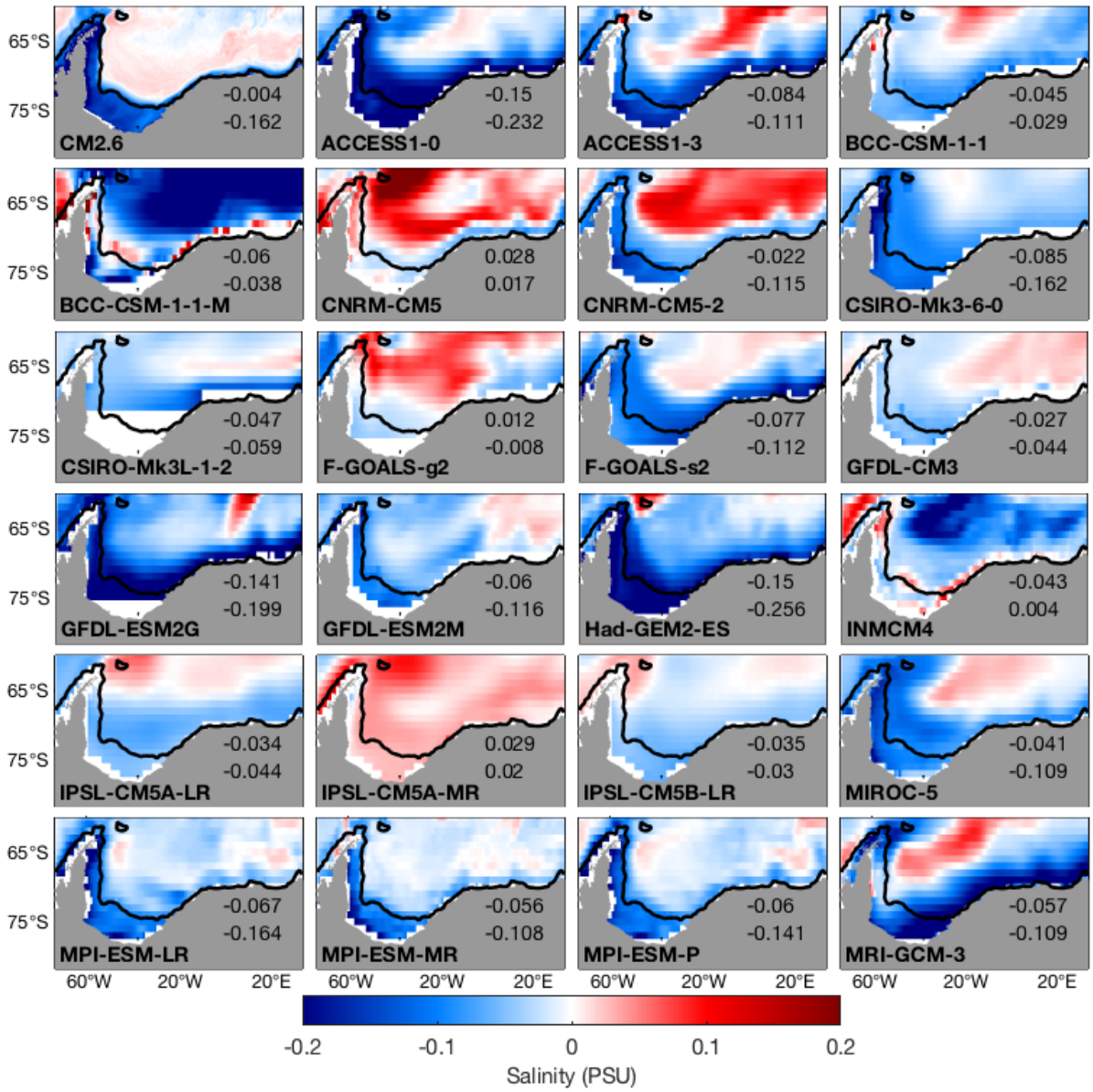

Figure 3–10: Depth average salinity change (0-1000 m; 1pctCO_2 minus piControl) with the 1000 m isobath (black contour) for all models for the Weddell Sea sector. The lower bold values on the continent are the depth averaged (0 - 1000) salinity change for the shelf region in the Weddell Sea (defined using the 1000 m isobath) whilst the upper values refer to the open ocean salinity change in the Weddell Sea for all models used.

open ocean regions in most CMIP5 models leads to the spreading of climate warming induced freshwater anomalies away from the coast and into the open ocean.

Hence, the absence of significant freshening in the open ocean region of the Weddell Sea in CM2.6 likely results in the continuation of the deep convection events and associated polynyas. In contrast, freshening and density changes in CMIP5 models display limited spatial distinction

Model	Shelf change WFO (Sv)	Open ocean change WFO (Sv)
CM2.6	0.0087	0.0032
ACCESS1-0	0.0061	0.0051
ACCESS1-3	0.0091	0.0047
CNRM-CM5	-0.0032	-0.0034
CNRM-CM5-2	0.0067	0.0063
GFDL-ESM2G	0.0074	0.0012
GFDL-ESM2M	0.0022	0.0015
GFDL-CM3	0.0053	0.0012
HadGEM2-ES	0.0083	0.0082
IPSL-CM5A-LR	0.0041	0.0018
IPSL-CM5A-MR	-0.0065	-0.0041
MIROC5	0.0038	0.0099
MPI-ESM-LR	0.0056	0.0011
MPI-ESM-MR	0.0034	0.0013
CMIP5 mean (std)	0.0056 (0.0021)	0.0038 (0.0032)

Table 3–4: Change in integrated water flux into the ocean (WFO) for the Weddell Sea shelf and open ocean regions. The CMIP5 model means are calculated using only models with positive WFO values.

between the shelf and open ocean regions likely resulting in a reduction of open ocean convection under climate change (Fig. 3–13 and Fig. 3–14).

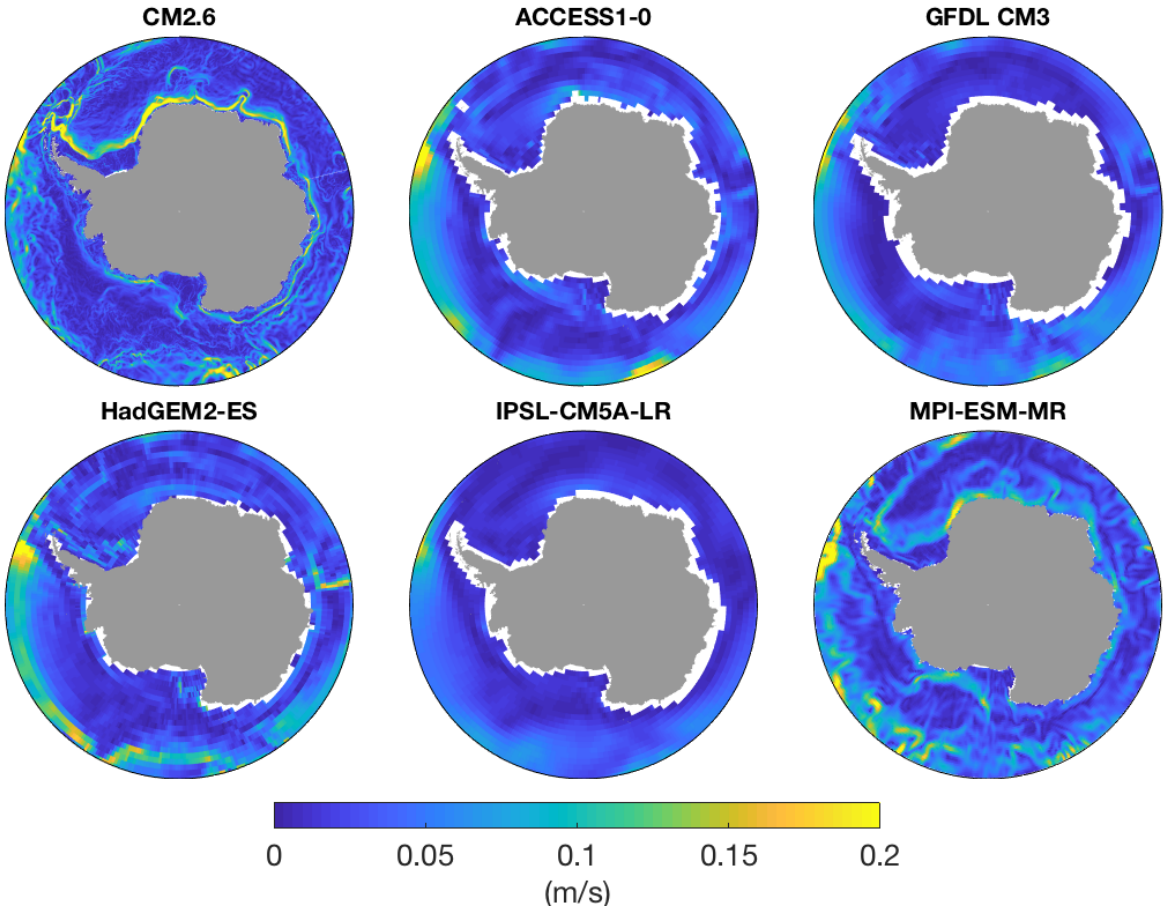

Figure 3–11: Depth averaged (0 - 1000 m) speed averaged over the control simulation.

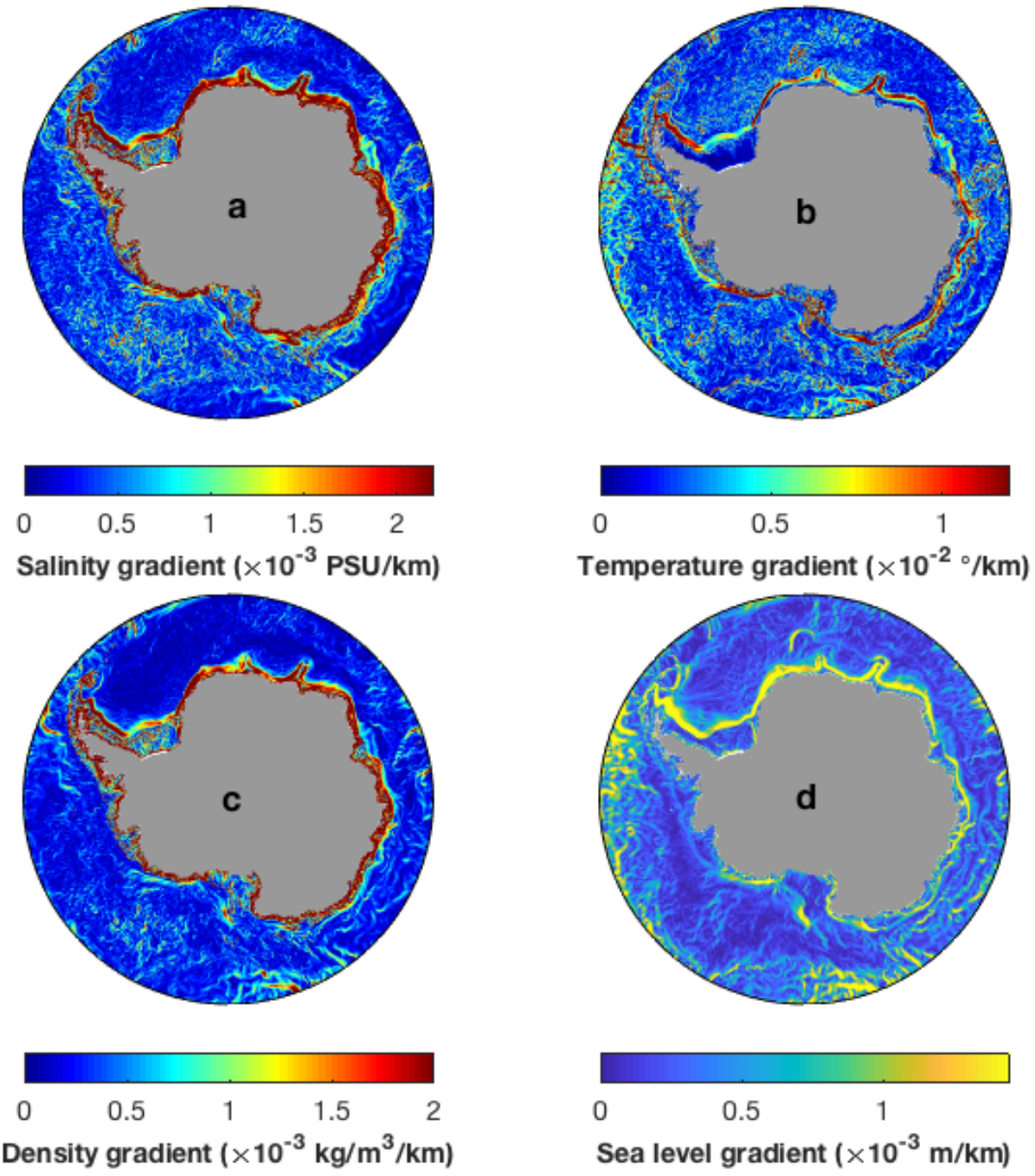

Figure 3–12: Magnitude of lateral gradient for CM2.6 in a) salinity (0 - 1000 m), b) potential temperature (0 - 1000 m), c) density (0 - 1000 m) and d) effective surface level averaged over the control for non-convective period (Table. 3–1).

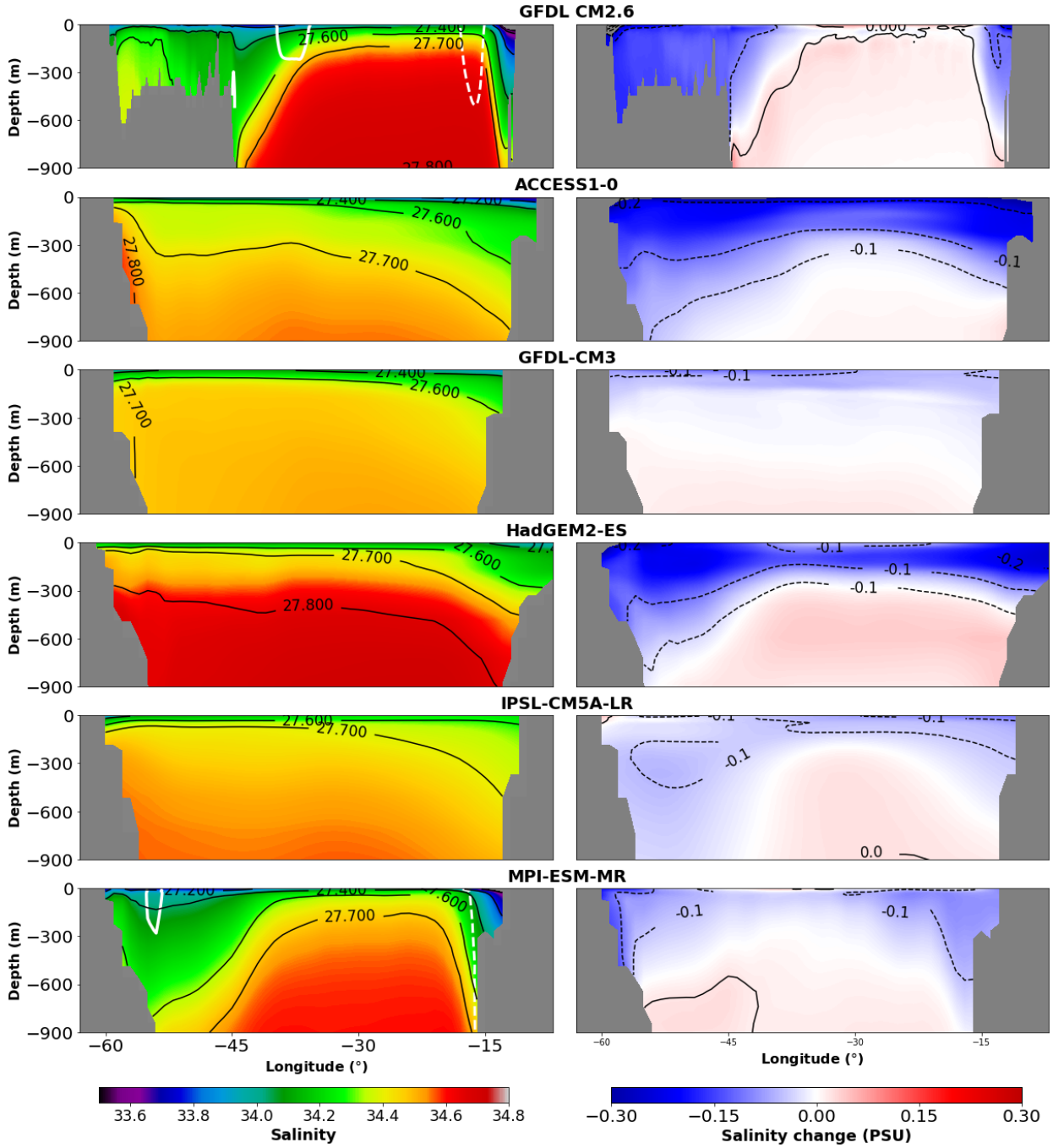

Figure 3–13: Salinity cross-sections at 71°S, across the central Weddell Sea (10-63°W). First column; control averaged salinity (shading), potential density referenced to the surface (σ_0 in kg/m^3; black lines) and ±0.08 m/s zonal velocity contours (in m/s; white lines) over the control. Plain velocity contours correspond to northward velocity and dashed velocity contours to southward velocity. Second column; change in salinity (shading) and σ_0 (black lines). Dashed lines correspond to negative values.

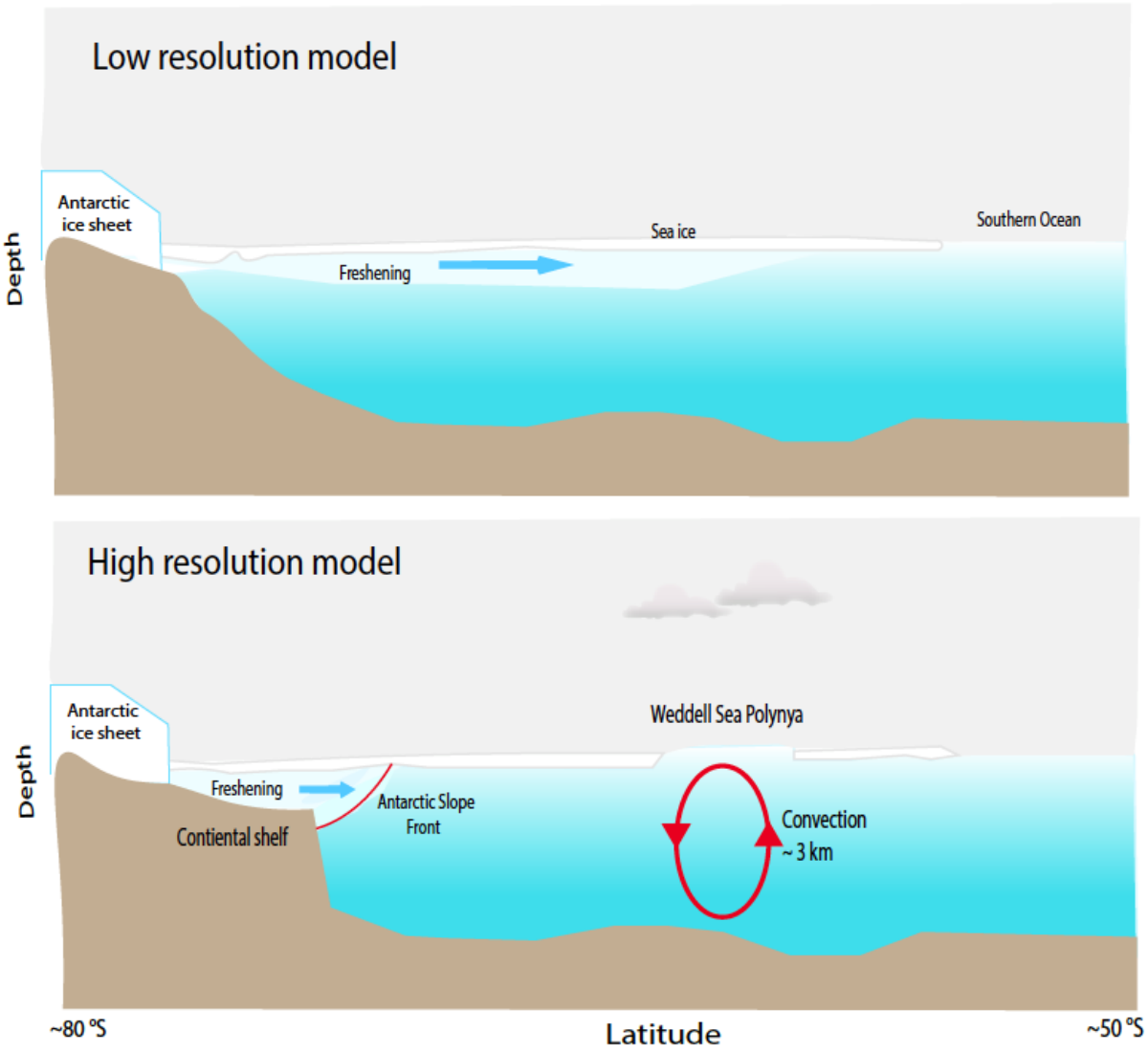

Figure 3–14: Conceptual model of the Weddell Sea Polynya under climate change for the low resolution models (CMIP5, top) and high resolution model (CM2.6, bottom).

4
Discussion

Using a large subset of climate models, we have found that the coarse resolution CMIP5 models show a cessation or slow down of convection events, in agreement with de Lavergne et al. (2014). In contrast, the high resolution CM2.6 shows a continuation of these events under climate change. The slow down of convection events in the CMIP5 models are shown to be caused by enhanced open ocean surface freshening and vertical stratification (Section 3.2). These results are consistent with previous studies focusing on the response of convection events to changes in salinity, vertical ocean stratification and freshwater fluxes (Martin et al., 2013; de Lavergne et al., 2014; Stössel et al., 2015).

4.1 Representation of the ASF and ASC in models

Despite generally exhibiting a high transient climate response over the 1pctCO_2 simulation compared to CMIP5 models (Winton et al. 2014; see Section 2.1.1), the occurrence and intensity of convection events in the high resolution CM2.6 is found to be largely unchanged between the piControl and 1pctCO_2 simulations. Namely, its change in open ocean salinity and convection area are indistinguishable from natural variability represented by the piControl. This absence of a significant change in response to the 1pctCO_2 forcing in CM2.6 is due to the ASF acting as a barrier to the transport of freshwater away from the shelf. To help assess the integrity of the modeled ASF and ASC, we here evaluate the ASC and ASF from CM2.6 and CMIP5 models as compared to that from the LLC_4320 model which simulates the ASF with high fidelity when compared to observations (Stewart et al. 2018; Section 2.1.3).

Comparison between CM2.6 and LLC_4320 reveals general agreement in ASC velocity and frontal structure (Fig. 4–1), though CM2.6 shows stronger (by approximately 0.1 m s^{-1}) surface zonal flow along the Southern Weddell Sea (Fig. 4–1 g,l) and surface meridional flow along the Western Weddell Sea (Fig. 4–2 g,l). In the Weddell Sea region, heavier density classes are able to access the shelf region in LLC_4320, whereas stronger isopycnal doming towards the continent

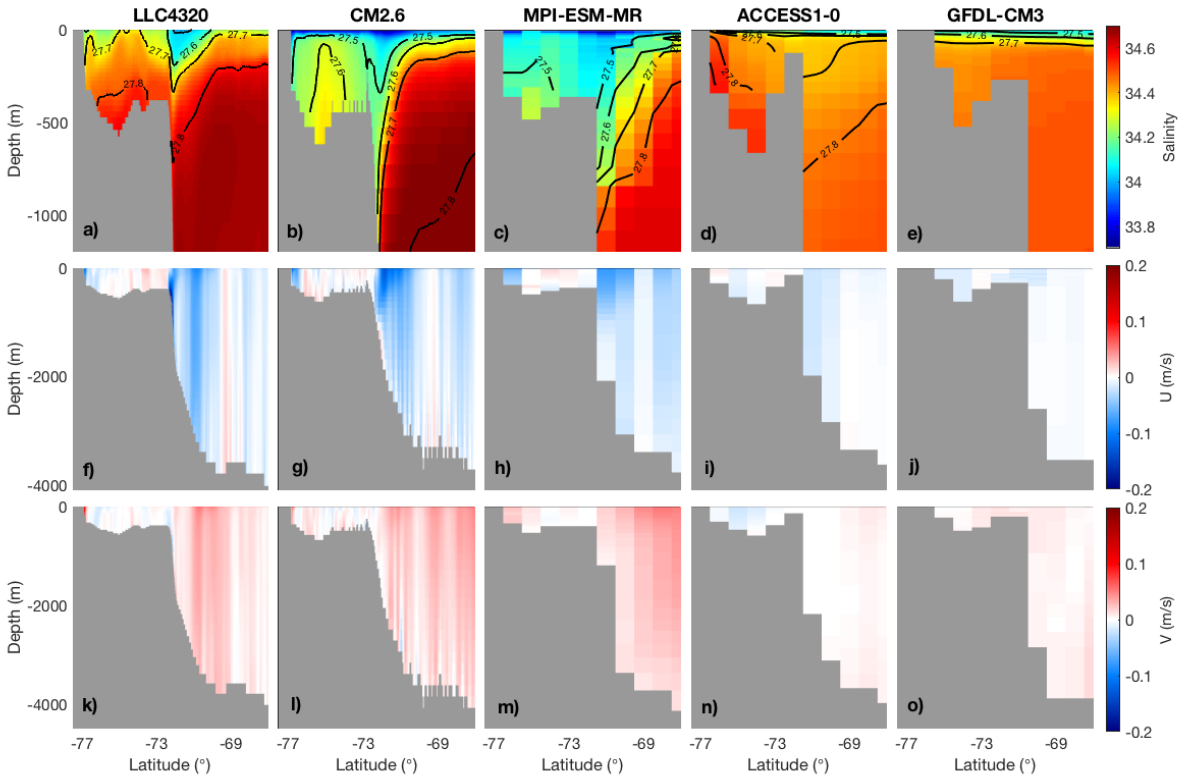

Figure 4–1: Comparison between modeled ASC and ASF for LLC4320 model (1/48°), CM2.6 (1/10°), MPI-ESM-MR (4/10°), ACCESS1-0 (1°) and GFDL-CM3 (1°). Cross sections at 50°W (Fig. 2-3) of (first row) salinity, (second row) zonal velocity (U) and (third row) meridional velocity (V). Labels on the black contours indicate potential densities referenced to the surface (in kg/m^3). Note the different depth range for the salinity cross sections (a-e) compared to velocity cross sections. For the CM2.6, MPI-ESM-MR, ACCESS1-0 and GFDL-CM3, variables are averaged over the full control simulation.

in CM2.6 isolates the lower shelf region from the open ocean. At the surface, where freshening propagates from the shelf to the open ocean region, CM2.6 and LLC_4320 have similar ASF structures, with fresh shelf water limited to approximately the same extent across the shelf (Fig. 4–1 a-b). In contrast, CMIP5 models are unable to capture the ASC (Fig. 4–1 h–j and m–o) and the associated ASF (Fig. 4–1 d,e) with the finer horizontal resolution (0.4° × 0.4°) MPI-ESM-MR being the exception. Yet, in MPI-ESM-MR, the representation of the ASC and ASF (Fig. 4–1 c,h,m) allows for limited representation of the salinity and density gradients across the shelf break compared to CM2.6 and LLC_4320.

Though there is an overall agreement between CM2.6 and LLC_4320, the ASF and ASC in CM2.6 may be too strong compared to observations as argued in Goddard et al. (2017), which

would lead to a too strong retention of freshwater over the shelf region. The too strong ASF and ASC in CM2.6 may be due to under-represented mesoscale eddy activity, which if resolved, would flatten isopycnals akin to the LLC_4320 simulation. CM2.6 may also simulate a too laminar ASF and ASC, which may lead to an overly strong dynamical barrier, whereas a more turbulent flow would allow the emission of mesoscale eddies hence contributing to the lateral transport of surface freshwater anomalies (Stewart and Thompson, 2015). In addition to mesoscale eddies, tides and dense overflows are thought to be critical components of cross-slope and cross-shelf exchange (Thompson et al., 2018). Strong tides in the central Weddell Seas should subdue cross-slope exchange, whereas the weaker tidal amplitudes in the western Weddell Sea should intensify cross-slope exchange (Beckmann and Pereira, 2003; Thompson et al., 2018). Dense water overflows directly affect the overlying stratification associated with the ASF (Baines, 2008). In CM2.6, dense water overflows are weak and do not exceed 1500 m, due to insufficient resolution on the horizontal leading to under-representation of mesoscale eddies and fine-scale topography (Dufour et al., 2017) and insufficient resolution on the vertical that does not allow for resolving dense downslope flow scales (Winton et al., 1998). Lack of full representation of mesoscale eddies, tides and dense water overflows, may therefore, alter the ability of CM2.6 in realistically capturing the ASF and associated cross-shelf freshwater exchange.

Even so, the general congruence between CM2.6 and LLC_4320 on the representation of the ASF in particular near the surface, and the inability of CMIP5 models in simulating the ASF and ASC suggest that CM2.6 may be closer to reality than CMIP5 models. If so, convection and associated WSP under climate change may well continue into the future as suggested by CM2.6 simulations, though the frequency and/or duration of the events could be altered. As only one member of each simulation is used in this analysis, caution should be taken on drawing any definitive conclusion. In particular, ensemble members run over longer time period would be needed to separate natural variability from the forced signal, and hence to confirm our results. Running large ensemble members of CM2.6 model is currently beyond modelling centers computational capabilities.

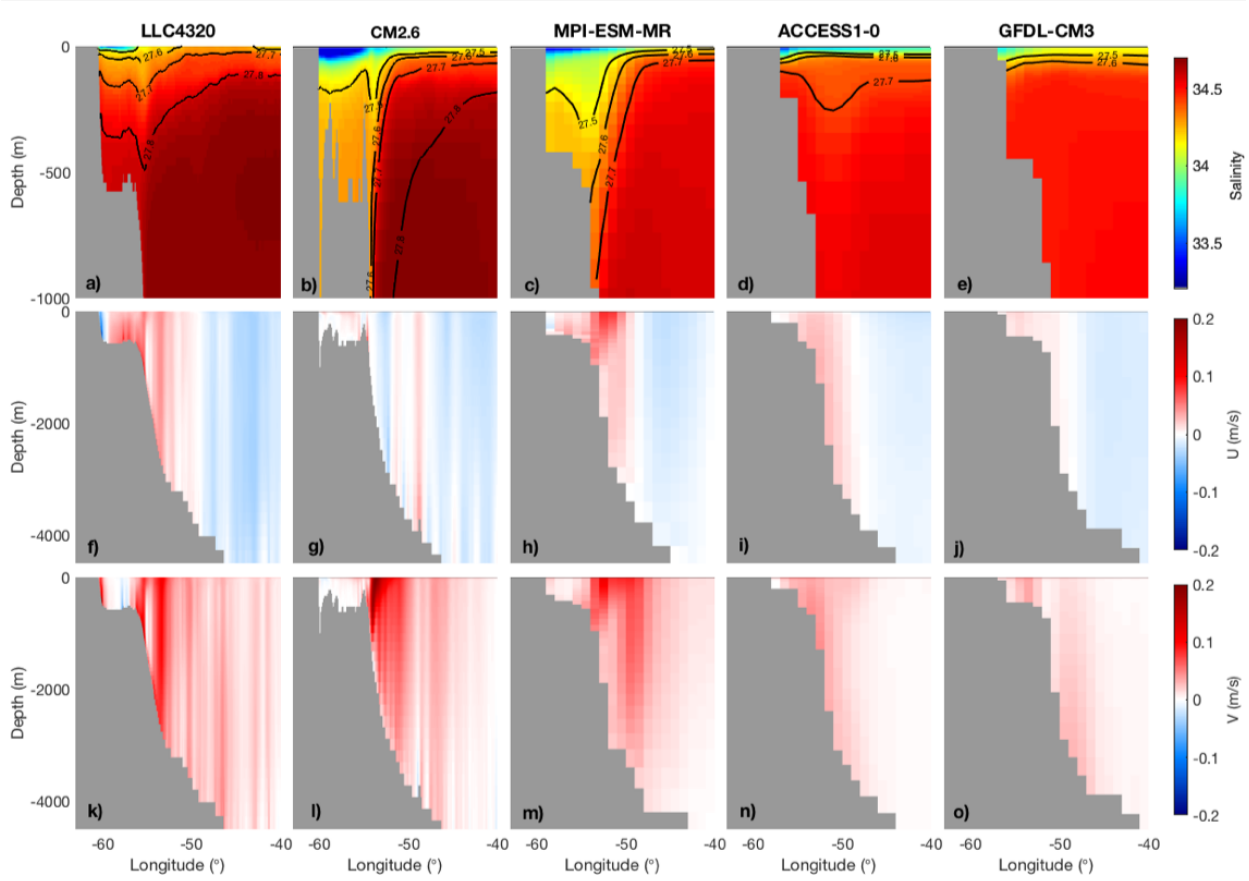

Figure 4–2: Comparison between modeled ASC and ASF for LLC4320 model (1/48°), CM2.6 (1/10°), MPI-ESM-MR (4/10°), ACCESS1-0 (1°) and GFDL-CM3 (1°). Cross sections at 65.5°S (Fig. 2-3) of (first row) salinity, (second row) zonal velocity (U) and (third row) meridional velocity (V). Labels on the black contours indicate potential densities referenced to the surface (in kg/m3). Note the different depth range for the salinity cross sections (a-e) compared to velocity cross sections. For the CM2.6, MPI-ESM-MR, ACCESS1-0 and GFDL-CM3, variables are averaged over the full control simulation.

In the future, freshening at the surface of the open-ocean region around Antarctica may therefore be constrained in scope due to the ASF and ASC, although some freshening may be expected in regions with an absence of the ASF and ASC. The ASC exists as a complex feature with multiple jets, and similar to other major frontal currents, its efficiency as a barrier to cross frontal transport is variable in both space and time (Bower et al., 1985). As such, following Thompson et al. (2018), we identify three regions of ASF and ASC strength in CM2.6: strong, moderate and weak. In regions where the ASF and ASC are very weak or even absent, such as along the West Antarctic Peninsula (Fig. 4–3) and Bellinghausen Sea, the freshening signal spreads beyond the shelf region at most depths (Fig. 4–4). In regions where the ASF and ASC

are of moderate strength, such as along the Indian Ocean sector of the Antarctic (Fig. 4–5), Ross Sea (Fig. 4–6) and Amundsen Sea (Fig. 4–7), a strong lateral density gradients across the shelf acts to constrain freshening at most depths. Finally, in regions of strong ASF and ASC, such as the Weddell Sea and Maud Rise regions, freshening is strictly constrained to the shelf region with little surface propagation of freshwater (see Section 3.3.2).

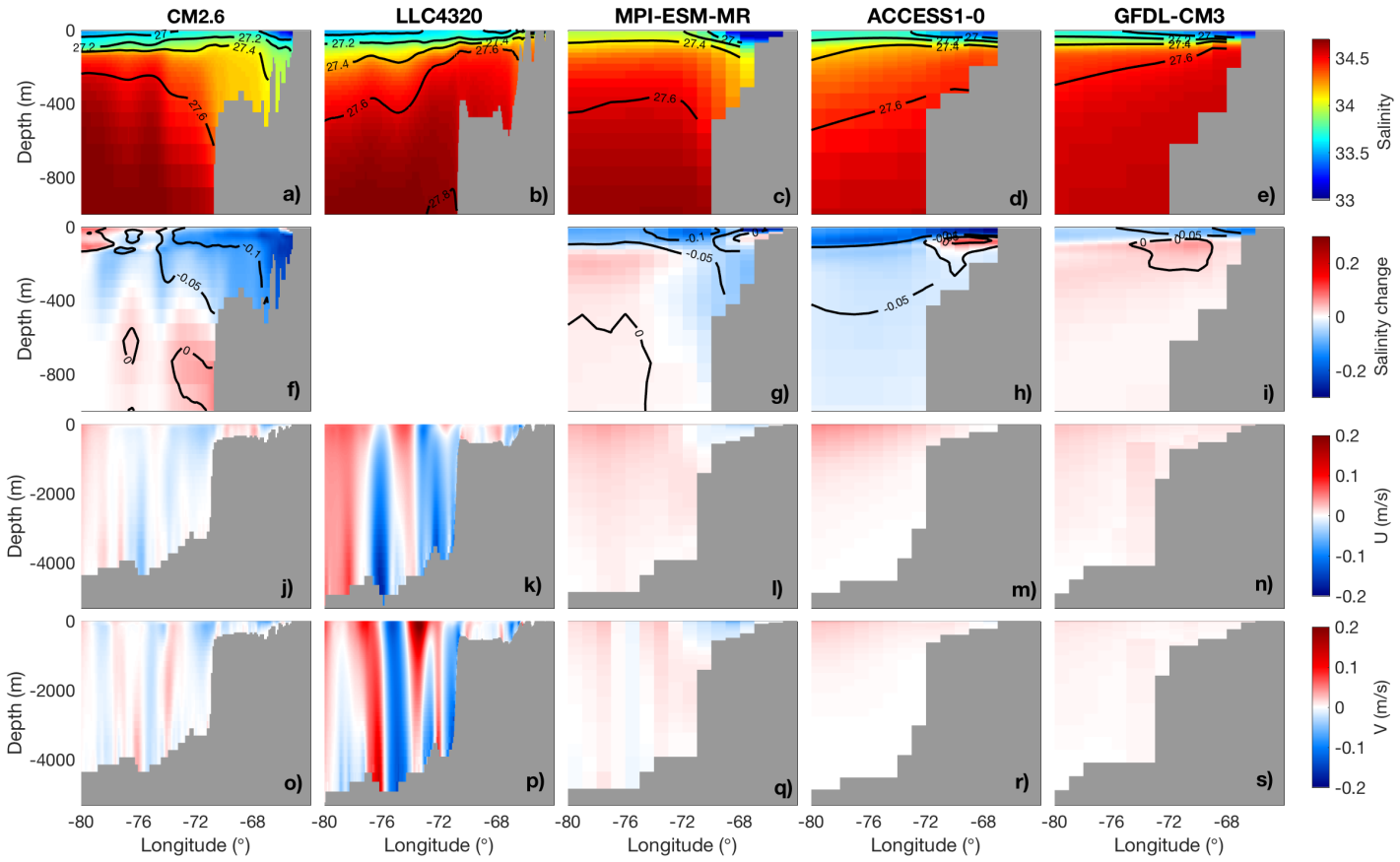

Figure 4–3: Comparison between modeled ASC and ASF for CM2.6 (1/10°), LLC4320 model (1/48°), MPI-ESM-MR (4/10°), ACCESS1-0 (1°) and GFDL-CM3 (1°). Cross sections of constant latitude at 66°S (Fig. 2-3) of (first row) salinity, (second row) salinity change, (third row) zonal velocity (U) and (fourth row) meridional velocity (V). Labels on the black contours indicate potential densities referenced to the surface (in kg/m^3). Note the different depth range for the salinity cross sections (a-i) compared to velocity cross sections. For the CM2.6, MPI-ESM-MR, ACCESS1-0 and GFDL-CM3, salinity and velocity variables are averaged over the full control simulation.

Spreading of the freshening signal in the absence of the ASF and ASC supports the mechanism proposed here in which the ASF and ASC are strong, freshening over the shelf does not spread to the open ocean region. This implies that, in sectors of the Southern Ocean offshore of regions

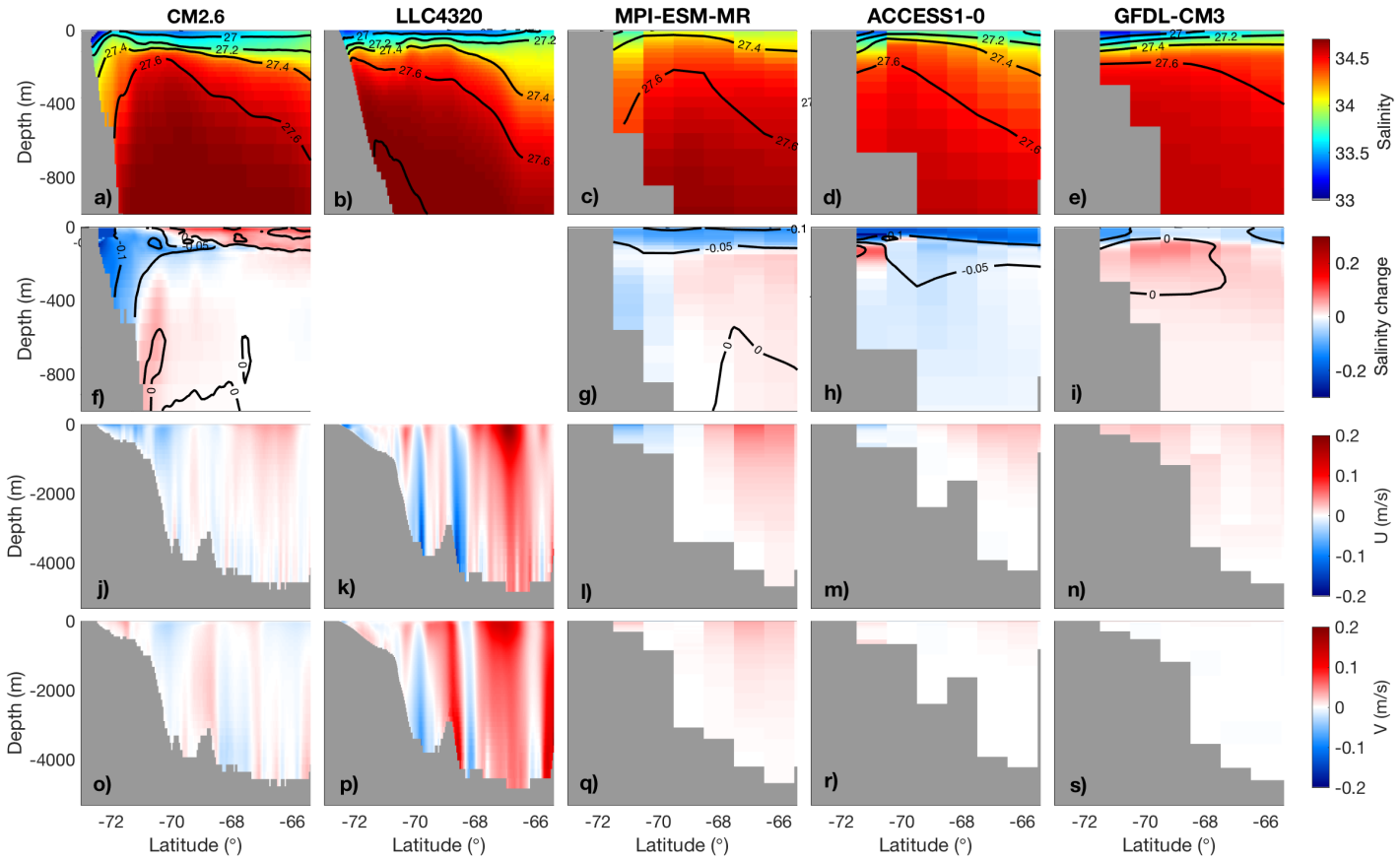

Figure 4–4: Comparison between modeled ASC and ASF for CM2.6 (1/10°), LLC4320 model (1/48°), MPI-ESM-MR (4/10°), ACCESS1-0 (1°) and GFDL-CM3 (1°). Cross sections at 90°W (Fig. 2-3) of (first row) salinity, (second row) salinity change, (third row) zonal velocity (U) and (fourth row) meridional velocity (V). Labels on the black contours indicate potential densities referenced to the surface (in kg/m^3). Note the different depth range for the salinity cross sections (a-i) compared to velocity cross sections. For the CM2.6, MPI-ESM-MR, ACCESS1-0 and GFDL-CM3, salinity and velocity variables are averaged over the full control simulation.

with a weak or absent ASF and ASC, a substantial decrease in salinity might be expected due to increased freshwater input on the shelf. In the absence of a dynamic barrier at the shelf break, this freshwater would propagate toward the open ocean. While the freshening in models between 68° S and 46° S is predominately attributed to precipitation-evaporation changes (see Section 3.3.1; de Lavergne et al., 2014), we found that the freshwater contributions from enhanced runoff from the Antarctic continent and sea ice flux changes to surface freshening are more dominant at higher latitude regions (< 68° S).

Similarly to Antarctic shelf circulation, strong boundary currents, including the East Greenland Current, West Greenland Current and Baffin Island Current, are found along the shelves of

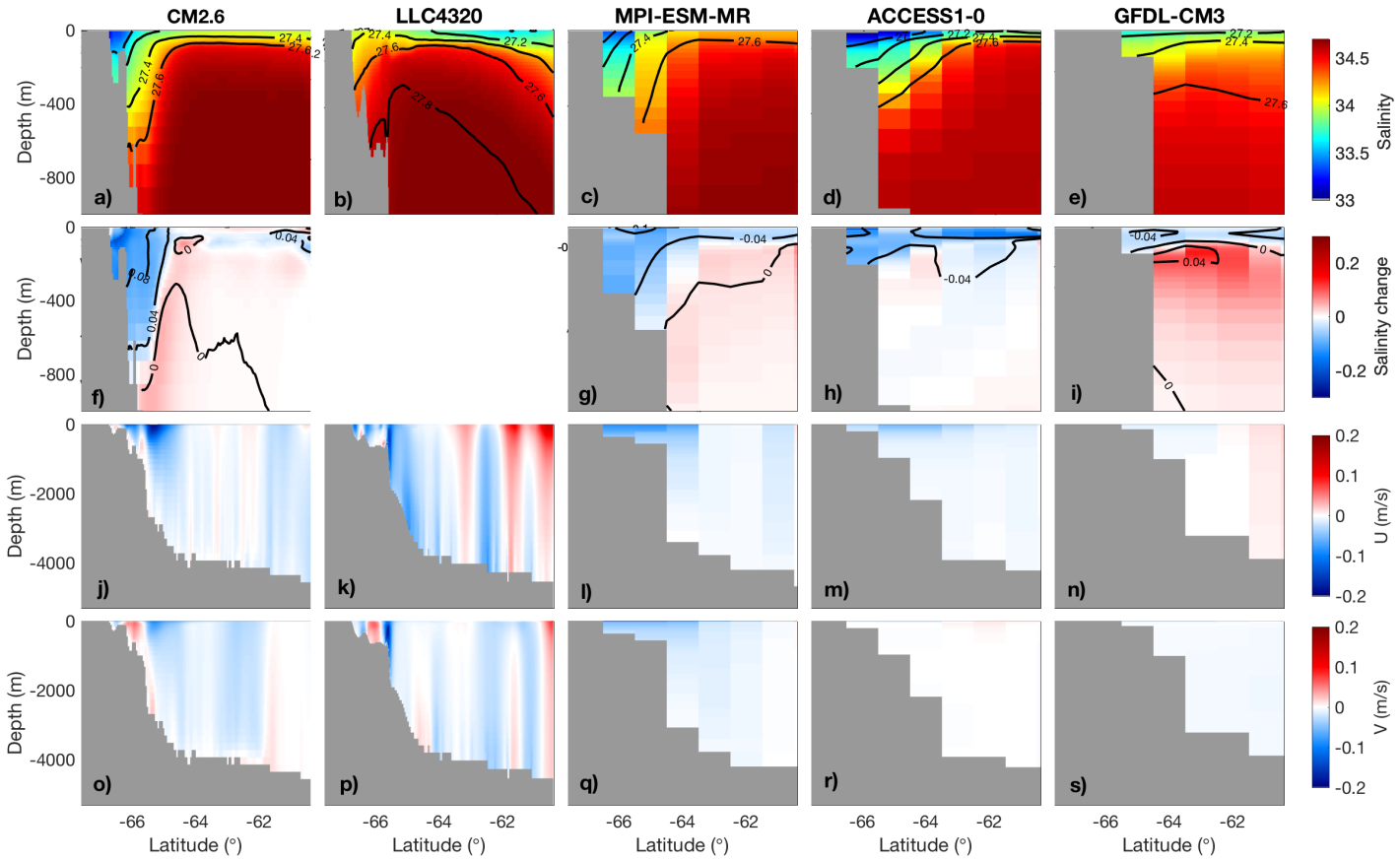

Figure 4–5: Comparison between modeled ASC and ASF for CM2.6 (1/10°), LLC4320 model (1/48°), MPI-ESM-MR (4/10°), ACCESS1-0 (1°) and GFDL-CM3 (1°). Cross sections at 90°E (Fig. 2-3) of (first row) salinity, (second row) salinity change, (third row) zonal velocity (U) and (fourth row) meridional velocity (V). Labels on the black contours indicate potential densities referenced to the surface (in kg/m^3). Note the different depth range for the salinity cross sections (a-i) compared to velocity cross sections. For the CM2.6, MPI-ESM-MR, ACCESS1-0 and GFDL-CM3, salinity and velocity variables are averaged over the full control simulation.

the polar North West Atlantic (Lazier and Wright, 1993). These boundary currents carry cold and fresh water and play a major role in mediating the transport of freshwater between the shelf and the open ocean (Marsh et al., 2010; Weijer et al., 2012; Dukhovskoy et al., 2016). Enhanced freshwater fluxes due to a melting Greenland ice sheet (Bamber et al., 2012; Enderlin et al., 2014) and changes in Arctic outflow (Peterson et al., 2002; Bamber et al., 2012; Dukhovskoy et al., 2016) are thus constrained between the shelf and open ocean regions by these currents, potentially impacting the sensitivity of Labrador Sea deep convection to climate change (Marsh et al., 2010; Weijer et al., 2012) with consequences for the strength of the Atlantic meridional overturning circulation (Stouffer et al., 2006; Rahmstorf et al., 2015). While the governing dynamics of the

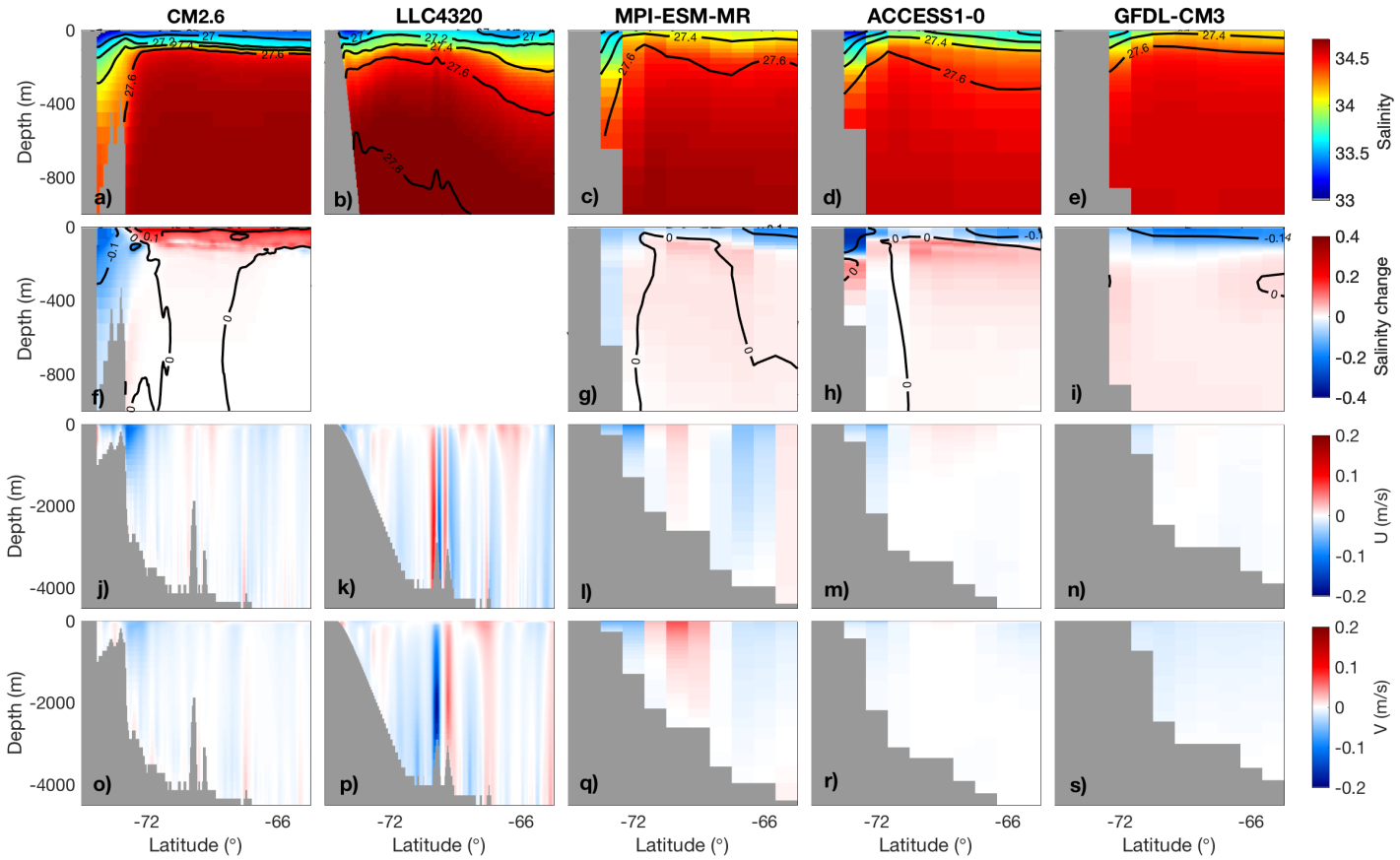

Figure 4–6: Comparison between modeled ASC and ASF for CM2.6 (1/10°), LLC4320 model (1/48°), MPI-ESM-MR (4/10°), ACCESS1-0 (1°) and GFDL-CM3 (1°). Cross sections at 130°W (Fig. 2-3) of (first row) salinity, (second row) salinity change, (third row) zonal velocity (U) and (fourth row) meridional velocity (V). Labels on the black contours indicate potential densities referenced to the surface (in kg/m^3). Note the different depth range for the salinity cross sections (a-i) compared to velocity cross sections. For the CM2.6, MPI-ESM-MR, ACCESS1-0 and GFDL-CM3, salinity and velocity variables are averaged over the full control simulation.

these Northern Hemisphere boundary currents and the ASC and ASF are more than likely to be different in nature, their effect on freshwater exchange and deep ocean convection would appear to be similar.

4.2 Conditions for reoccurrence of the WSP in the future

In 2016 and 2017, a large polynya opened at the Maud Rise. Though this event did not develop into a fully formed open ocean WSP, it was the largest event observed since 1980 (Cheon and Gordon, 2019). The opening of the Maud Rise polynyas of 2016 and 2017 has been attributed to polar cyclones (Campbell et al., 2019; Francis et al., 2019) which are expected to intensify and to shift southward into the future (Chang et al., 2012). Autonomous profiling float observations of

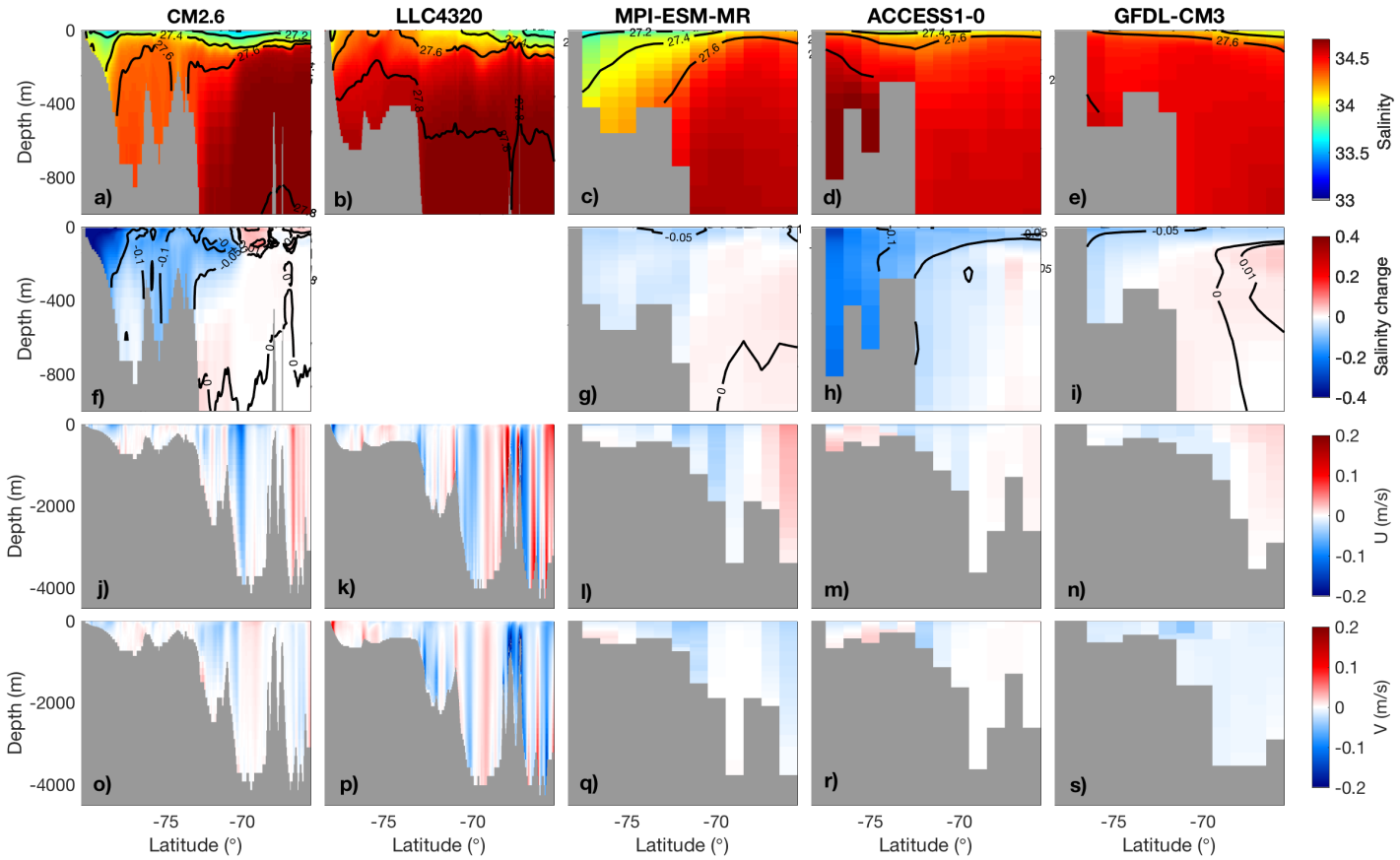

Figure 4–7: Comparison between modeled ASC and ASF for CM2.6 (1/10°), LLC4320 model (1/48°), MPI-ESM-MR (4/10°), ACCESS1-0 (1°) and GFDL-CM3 (1°). Cross sections at 180°W (Fig. 2-3) of (first row) salinity, (second row) salinity change, (third row) zonal velocity (U) and (fourth row) meridional velocity (V). Labels on the black contours indicate potential densities referenced to the surface (in kg/m^3). Note the different depth range for the salinity cross sections (a-i) compared to velocity cross sections. For the CM2.6, MPI-ESM-MR, ACCESS1-0 and GFDL-CM3, salinity and velocity variables are averaged over the full control simulation.

these recent events has also revealed that intense heat loss drove deep overturning and wind-driven upwelling weakened haline stratification in the upper ocean (Campbell et al., 2019). Combined, these changes in intensity and position of winds and polar cyclones may encourage the formation of Maud Rise polynyas that could in turn evolve into full WSPs.

Furthermore, the observed positive trend in the SAM (Thompson et al. 2000; Thompson and Solomon 2002; Gillett and Thompson 2003; Marshall 2003; Marshall et al. 2004) is projected to continue in the future as greenhouse gas concentrations keep rising (Thompson et al., 2011). Positive phases of the SAM correspond to a strengthening and a poleward shift of the SH westerlies (Kushner et al., 2001; Fyfe et al., 2007; Thompson et al., 2011) which increase negative wind stress

curl and the Weddell Sea Gyre within the Weddell Sea, activating mesoscale Weddell Deep Water eddies in the vicinity of Maud Rise and potentially promoting polynya events (Cheon and Gordon, 2019). In contrast to this dynamic effect, the positive trend in the SAM, which correlates inversely with salinity in the Weddell Sea, is thought to have resulted in fresh surface waters that could have hindered the transition of the Maud Rise polynyas to a full WSP in 2017 (Cheon and Gordon, 2019), and can potentially continue to impede WSP formation into the future.

As more heat is brought poleward by the Weddell Sea Gyre, fed by the warming Antarctic Circumpolar Current (Gille, 2002) and by the poleward heat transport by mesoscale eddies (e.g. Screen et al., 2009), and as stratification is enhanced (even moderately; see previous section), the SHR may build up for a longer time (see Fig. 3–2 and 3–4). So, should convection be initiated, it could last longer or be more vigorous. This hypothesis is supported by CM2.6, which simulates a polynya as doubling of the atmospheric CO_2 is reached in the 1pctCO_2 simulation that is marginally longer and larger than the polynya developing at the end of the piControl simulation, which we posit is due to the increase in the SHR under climate change (Fig. 3–2). The build up of the SHR is also very clear in the CMIP5 models (Fig. 3–4). This build up has been suggested by the regional warming of the Weddell Deep Water quantified at 0.034° C per decade from 1977 to 2001 along sections of the Weddell Sea (Gille, 2002; Smedsrud, 2005), likely due to the warming ACC feeding the Weddell Gyre (Orsi et al., 1999) which resulted in the subsequent enhanced convergence of heat. Hence, the intensity and duration of future convection events may be more intense and over longer duration than that of the 1970's WSP.

A major caveat in our results based on CMIP5 and CM2.6 models is related to the lack of active ice sheet components that simulate the ice sheets and ice shelves melt from the Antarctica, both great contributors to the observed freshening (Jacobs et al., 2002; Flato et al., 2013; Bronselaer et al., 2018). Hence, freshening is likely underestimated in CMIP5 and CM2.6 models. Using the GFDL-ESM2M model, Bronselaer et al. (2018) show that adding meltwater representative of ice sheet melt to the surface ocean within 3° of the coast increases the formation of Antarctic sea ice and warms the subsurface ocean around the Antarctic coast. It is thus expected that the stratification around Antarctica would be significantly affected by the addition of an

active ice sheet component in CMIP5 and CM2.6 models. However, our results show that an improved representation of shelf ocean circulation in coarse resolution climate models, akin to CM2.6, would substantially limit the propagation of this additional meltwater from the coastal region, thus constraining the associated effects to the Antarctic coasts.

In sum, future occurrence of the WSP can be conceptualized as a competition between the stabilizing effect of relatively fresh surface waters, driven by surface freshening and thermodynamic effects associated with positive SAM phases, and destabilizing effect of convection triggers, such as frequency of polar cyclones, Weddell Sea gyre strength and meridional heat transport. If polynya triggers are not stronger nor more frequent and a substantial increase in open ocean stratification is able to occur, a slow down or cessation of open ocean polynya in the Weddell Sea may well be expected. If triggers become stronger and more frequent with limited open ocean freshening, which is suggested by our analysis of CM2.6 and the expected strengthening of polynya triggers, re-occurrence of WSPs may otherwise be expected into the future.

5
Conclusion

In this study, we investigated the occurrence of the Weddell Sea Polynya (WSP) under climate change by comparing a large subset of the coarse resolution CMIP5 models with the high resolution CM2.6 climate model. Our key findings are as follows.

- Under climate change, CM2.6 forms WSPs with similar timing and duration as under pre-industrial forcing, whereas CMIP5 models show either a cessation or slowdown of these events under climate change.
- The cessation of convection in CMIP5 models is due to open ocean surface freshening. Surface freshening in the models is driven by enhanced precipitation over evaporation north of 68°S, and runoff from the Antarctic continent and sea ice flux changes south of 68°S.
- The circumpolar Antarctic Slope Current and associated Antarctic Slope Front are not resolved by the coarse resolution CMIP5 models, whereas they are more realistically represented in CM2.6. This improved representation of shelf circulation in CM2.6 confines the coastal freshening to the shelf. As a result, CMIP5 models are prone to large scale open ocean freshening, leading to a slow down, or even cessation, of WSP events, whereas CM2.6 is not.

Hence, our results suggest a continuation of the open ocean convection events and associated polynyas in the future. To allow for more accurate projections of these important climate events, an improved representation of shelf ocean circulation in climate models is needed.

6 References

Bibliography

Baines, P. G., 2008: Mixing in downslope flows in the ocean - plumes versus gravity currents. *Atmosphere-Ocean*, **46 (4)**, 405–419, doi:10.3137/ao.460402.

Bamber, J., M. van den Broeke, J. Ettema, J. Lenaerts, and E. Rignot, 2012: Recent large increases in freshwater fluxes from Greenland into the North Atlantic. *Geophysical Research Letters*, **39 (19)**, doi:10.1029/2012GL052552.

Beadling, R. L., J. L. Russell, R. J. Stouffer, P. J. Goodman, and M. Mazloff, 2019: Assessing the quality of southern ocean circulation in cmip5 aogcm and earth system model simulations. *J. Climate*, **32 (18)**, 5915–5940, doi:10.1175/JCLI-D-19-0263.1.

Beckmann, A., and A. F. Pereira, 2003: Lateral tidal mixing in the antarctic marginal seas. *Ocean Dynamics*, **53 (1)**, 21–26, doi:10.1007/s10236-002-0020-9.

Bower, A. S., H. T. Rossby, and J. L. Lillibridge, 1985: The gulf stream—barrier or blender? *Journal of Physical Oceanography*, **15 (1)**, 24–32, doi:10.1175/1520-0485(1985)015<0024:TGSOB>2.0.CO;2.

Boyer, T., and Coauthors, 2018: World ocean database 2018. **NOAA Atlas NESDIS 87**, doi:10.7289/V5NZ85MT.

Bracegirdle, T. J., E. Shuckburgh, J. Sallee, Z. Wang, A. J. S. Meijers, N. Bruneau, T. Phillips, and L. J. Wilcox, 2013: Assessment of surface winds over the atlantic, indian, and pacific ocean sectors of the southern ocean in cmip5 models: historical bias, forcing response, and state dependence. *Journal of Geophysical Research: Atmospheres*, **118 (2)**, 547–562, doi:10.1002/jgrd.50153.

Bronselaer, B., M. Winton, S. Griffies, W. Hurlin, K. Rodgers, O. Sergienko, R. Stouffer, and J. Russell, 2018: Change in future climate due to antarctic meltwater. *Nature*, **564**, doi:10.1038/s41586-018-0712-z.

Campbell, E., E. Wilson, G. Moore, S. Riser, C. Brayton, M. Mazloff, and L. Talley, 2019: Antarctic offshore polynyas linked to southern hemisphere climate anomalies. *Nature*, **570**, 1–7, doi:10.1038/s41586-019-1294-0.

Carsey, F. D., 1980: Microwave observation of the weddell polynya. *Mon. Wea. Rev.*, **108 (12)**, 2032–2044, doi:10.1175/1520-0493(1980)108<2032:MOOTWP>2.0.CO;2.

Chang, E. K. M., Y. Guo, and X. Xia, 2012: Cmip5 multimodel ensemble projection of storm track change under global warming. *Journal of Geophysical Research: Atmospheres*, **117 (D23)**, doi:10.1029/2012JD018578.

Cheon, W., and A. Gordon, 2019: Open-ocean polynyas and deep convection in the southern ocean. *Scientific Reports*, **9**, doi:10.1038/s41598-019-43466-2.

Cheon, W. G., Y.-G. Park, J. R. Toggweiler, and S.-K. Lee, 2014: The relationship of weddell polynya and open-ocean deep convection to the southern hemisphere westerlies. *Journal of Physical Oceanography*, **44 (2)**, 694–713, doi:10.1175/JPO-D-13-0112.1.

Comiso, J. C., and A. L. Gordon, 1987: Recurring polynyas over the cosmonaut sea and the maud rise. *J. Geophys. Res.*, **92 (C3)**, 2819–2833, doi:10.1029/JC092iC03p02819.

Conkright, M., R. Locarnini, H. Garcia, T. O'Brien, T. Boyer, C. Stephens, and J. Antonov, 2002: World ocean atlas 2001: Objective analyses, data statistics, and figures, cd-rom documentation. *Internal Rep.*, **17**.

de Boyer Montégut, C., G. Madec, A. S. Fischer, A. Lazar, and D. Iudicone, 2004: Mixed layer depth over the global ocean: An examination of profile data and a profile-based climatology. *J. Geophys. Res.: Oceans*, **109 (C12)**, doi:10.1029/2004JC002378.

de Lavergne, C., J. B. Palter, E. D. Galbraith, R. Bernardello, and I. Marinov, 2014: Cessation of deep convection in the open Southern Ocean under anthropogenic climate change. *Nat. Clim. Change*, **4**, 278, doi:10.1038/nclimate2132.

Dee, D. P., and Coauthors, 2011: The era-interim reanalysis: configuration and performance of the data assimilation system. *Q. J. R. Meteorol. Soc.*, **137 (656)**, 553–597, doi:10.1002/qj.828.

Delworth, T. L., and Coauthors, 2012: Simulated climate and climate change in the gfdl cm2.5 high-resolution coupled climate model. *Journal of Climate*, **25 (8)**, 2755–2781, doi: 10.1175/JCLI-D-11-00316.1.

Dufour, C. O., A. K. Morrison, S. M. Griffies, I. Frenger, H. Zanowski, and M. Winton, 2017: Preconditioning of the Weddell Sea Polynya by the Ocean Mesoscale and Dense Water Overflows. *Journal of Climate*, **30 (19)**, 7719–7737, doi:10.1175/JCLI-D-16-0586.1.

Dukhovskoy, D. S., and Coauthors, 2016: Greenland freshwater pathways in the sub-Arctic Seas from model experiments with passive tracers. *Journal of Geophysical Research: Oceans*, **121 (1)**, 877–907, doi:10.1002/2015JC011290.

ECMWF, 2011: European centre for medium-range weather forecasts.

Enderlin, E. M., I. M. Howat, S. Jeong, M.-J. Noh, J. H. van Angelen, and M. R. van den Broeke, 2014: An improved mass budget for the Greenland ice sheet. *Geophysical Research Letters*, **41 (3)**, 866–872, doi:10.1002/2013GL059010.

Flato, G., and Coauthors, 2013: *Evaluation of Climate Models. In: Climate Change 2013: The Physical Science Basis. Contribution of Working Group I to the Fifth Assess- ment Report of the Intergovernmental Panel on Climate Change [Stocker, T.F., D. Qin, G.-K. Plattner, M. Tignor, S.K. Allen, J. Boschung, A. Nauels, Y. Xia, V. Bex and P.M. Midgley (eds.)]*., 741–882. Cambridge University Press, Cambridge, UK, doi:10.1017/CBO9781107415324.020.

Fox-Kemper, B., and Coauthors, 2011: Parameterization of mixed layer eddies. iii: Implementation and impact in global ocean climate simulations. *Ocean Modell.*, **39**, 61–78, doi: 10.1016/j.ocemod.2010.09.002.

Francis, D., C. Eayrs, J. Cuesta, and D. Holland, 2019: Polar cyclones at the origin of the reoccurrence of the maud rise polynya in austral winter 2017. *Journal of Geophysical Research: Atmospheres*, **124 (10)**, 5251–5267, doi:10.1029/2019JD030618.

Fyfe, J. C., O. A. Saenko, K. Zickfeld, M. Eby, and A. J. Weaver, 2007: The role of poleward-intensifying winds on southern ocean warming. *J. Climate*, **20 (21)**, 5391–5400, doi: 10.1175/2007JCLI1764.1.

Gille, S. T., 2002: Warming of the southern ocean since the 1950s. *Science*, **295 (5558)**, 1275–1277, doi:10.1126/science.1065863.

Gillett, N. P., and D. W. J. Thompson, 2003: Simulation of recent southern hemisphere climate change. *Science*, **302 (5643)**, 273–275, doi:10.1126/science.1087440.

Goddard, P. B., C. O. Dufour, J. Yin, S. M. Griffies, and M. Winton, 2017: Co2-induced ocean warming of the antarctic continental shelf in an eddying global climate model. *J. Geophys. Res.: Oceans*, **122 (10)**, 8079–8101, doi:10.1002/2017JC012849.

Gordon, A., 1982: Weddell deep water variability. *J. Mar. Res.*, **40**, 199–217.

Gordon, A. L., 1978: Deep antarctic convection west of maud rise. *J. Phys. Oceanogr.*, **8 (4)**, 600–612, doi:10.1175/1520-0485(1978)008<0600:DACWOM>2.0.CO;2.

Gordon, A. L., M. Visbeck, and J. C. Comiso, 2007: A possible link between the weddell polynya and the southern annular mode. *J. Climate*, **20 (11)**, 2558–2571, doi:10.1175/JCLI4046.1.

Gouretski, V., 2018: Woce-Argo Global Hydrographic Climatology. *Ocean Science Discussions*, 1–30, doi:10.5194/os-2018-34.

Griffies, S. M., and Coauthors, 2015: Impacts on ocean heat from transient mesoscale eddies in a hierarchy of climate models. *J. Climate*, **28 (3)**, 952–977, doi:10.1175/JCLI-D-14-00353.1.

Hallberg, R., 2013: Using a resolution function to regulate parameterizations of oceanic mesoscale eddy effects. *Ocean Modelling*, **72**, 92 – 103, doi:https://doi.org/10.1016/j.ocemod.2013.08.007.

Haumann, F. A., N. Gruber, M. Münnich, I. Frenger, and S. Kern, 2016: Antarctic sea-ice freshwater fluxes associated with freezing, transport, and melting. ETH Zurich, doi: http://dx.doi.org/10.16904/8.

Heuzé, C., K. J. Heywood, D. P. Stevens, and J. K. Ridley, 2013: Southern ocean bottom water characteristics in cmip5 models. *Geophys. Res. Lett.*, **40 (7)**, 1409–1414, doi:10.1002/grl.50287.

Heywood, K. J., and Coauthors, 2014: Ocean processes at the antarctic continental slope. *Philos. Trans. R. Soc., A*, **372 (2019)**, 20130 047, doi:10.1098/rsta.2013.0047.

Holland, D. M., 2001: Explaining the weddell polynya - a large ocean eddy shed at maud rise. *Science*, **292 (5522)**, 1697–1700, doi:10.1126/science.1059322.

Jacobs, S. S., 1991: On the nature and significance of the antarctic slope front. *Mar. Chem.*, **35 (1)**, 9 – 24, doi:https://doi.org/10.1016/S0304-4203(09)90005-6, biochemistry and circulation of water masses in the Southern Ocean.

Jacobs, S. S., C. F. Giulivi, and P. A. Mele, 2002: Freshening of the ross sea during the late 20th century. *Science*, **297 (5580)**, 386–389, doi:10.1126/science.1069574.

Jena, B., M. Ravichandran, and J. Turner, 2019: Recent reoccurrence of large open-ocean polynya on the maud rise seamount. *Geophys. Res. Lett.*, **46 (8)**, 4320–4329, doi:10.1029/2018GL081482.

Klinger, B. A., J. Marshall, and U. Send, 1996: Representation of convective plumes by vertical adjustment. *J. Geophys. Res.: Oceans*, **101 (C8)**, 18 175–18 182, doi:10.1029/96JC00861.

Kurtakoti, P., M. Veneziani, A. Stössel, and W. Weijer, 2018: Preconditioning and formation of maud rise polynyas in a high-resolution earth system model. *J. Climate*, **31 (23)**, 9659–9678, doi:10.1175/JCLI-D-18-0392.1.

Kushner, P. J., I. M. Held, and T. L. Delworth, 2001: Southern hemisphere atmospheric circulation response to global warming. *Journal of Climate*, **14 (10)**, 2238–2249, doi:10.1175/1520-0442(2001)014<0001:SHACRT>2.0.CO;2.

Large, W. G., J. C. McWilliams, and S. C. Doney, 1994: Oceanic vertical mixing: A review and a model with a nonlocal boundary layer parameterization. *Rev. Geophys.*, **32 (4)**, 363–403, doi:10.1029/94RG01872.

Lazier, J. R. N., and D. G. Wright, 1993: Annual Velocity Variations in the Labrador Current. *Journal of Physical Oceanography*, **23 (4)**, 659–678, doi:10.1175/1520-0485(1993)023<0659:AVVITL>2.0.CO;2.

Lindsay, R., D. Holland, and R. Woodgate, 2004: Halo of low ice concentration observed over the maud rise seamount. *Geophys. Res. Lett.*, **311**, doi:10.1029/2004GL019831.

Marsh, R., D. Desbruyères, J. L. Bamber, B. A. de Cuevas, A. C. Coward, and Y. Aksenov, 2010: Short-term impacts of enhanced Greenland freshwater fluxes in an eddy-permitting ocean model. *Ocean Science*, **6 (3)**, 749–760, doi:10.5194/os-6-749-2010.

Marshall, G. J., 2003: Trends in the southern annular mode from observations and reanalyses. *Journal of Climate*, **16 (24)**, 4134–4143, doi:10.1175/1520-0442(2003)016<4134:TITSAM>2.0.CO;2.

Marshall, G. J., P. A. Stott, J. Turner, W. M. Connolley, J. C. King, and T. A. Lachlan-Cope, 2004: Causes of exceptional atmospheric circulation changes in the southern hemisphere. *Geophysical Research Letters*, **31 (14)**, doi:10.1029/2004GL019952.

Martin, T., W. Park, and M. Latif, 2013: Multi-centennial variability controlled by southern ocean convection in the kiel climate model. *Climate Dyn.*, **40 (7)**, 2005–2022, doi:10.1007/s00382-012-1586-7.

Martinson, D. G., P. D. Killworth, and A. L. Gordon, 1981: A convective model for the weddell polynya. *J. Phys. Oceanogr.*, **11 (4)**, 466–488, doi:10.1175/1520-0485(1981)011<0466:ACMFTW>2.0.CO;2.

Melling, H., Y. Gratton, and G. Ingram, 2001: Ocean circulation within the north water polynya of baffin bay. *Atmosphere-Ocean*, **39 (3)**, 301–325, doi:10.1080/07055900.2001.9649683.

Moore, G., K. Alverson, and I. Renfrew, 2002: A reconstruction of the air–sea interaction associated with the weddell polynya. *Journal of Physical Oceanography*, **32**, 1685–1698, doi:10.1175/1520-0485(2002)032<1685:arotas>2.0.co;2.

Morales Maqueda, M. A., A. J. Willmott, and N. R. T. Biggs, 2004: Polynya dynamics: a review of observations and modeling. *Reviews of Geophysics*, **42 (1)**, doi:10.1029/2002RG000116.

Murray, R. J., 1996: Explicit generation of orthogonal grids for ocean models. *J. Comput. Phys.*, **126 (2)**, 251–273, doi:10.1006/jcph.1996.0136.

Orsi, A., G. Johnson, and J. Bullister, 1999: Circulation, mixing, and production of Antarctic Bottom Water. *Progress in Oceanography*, **43 (1)**, 55 – 109, doi:https://doi.org/10.1016/S0079-6611(99)00004-X.

Parkinson, C., 2014: Seasonality of southern ocean sea ice. Boulder, Colorado USA. NASA National Snow and Ice Data Center Distributed Active Archive Center, doi:10.5067/W2PKTWMTY0TP.

Pedlosky, J., 1987: *Geophysical Fluid Dynamics*.

Peterson, B. J., R. M. Holmes, J. W. McClelland, C. J. Vörösmarty, R. B. Lammers, A. I. Shiklomanov, I. A. Shiklomanov, and S. Rahmstorf, 2002: Increasing River Discharge to the Arctic Ocean. *Science*, **298 (5601)**, 2171–2173, doi:10.1126/science.1077445.

Rahmstorf, S., J. Box, G. Feulner, M. Mann, A. Robinson, S. Rutherford, and E. Schaffernicht, 2015: Exceptional twentieth-Century slowdown in Atlantic Ocean overturning circulation. *Nature Climate Change*, **5**, doi:10.1038/nclimate2554.

Rayner, N. A., D. E. Parker, E. B. Horton, C. K. Folland, L. V. Alexander, D. P. Rowell, E. C. Kent, and A. Kaplan, 2003: Global analyses of sea surface temperature, sea ice, and night marine air temperature since the late nineteenth century. *Journal of Geophysical Research: Atmospheres*, **108 (D14)**, doi:10.1029/2002JD002670.

Rocha, C. B., T. K. Chereskin, S. T. Gille, and D. Menemenlis, 2016: Mesoscale to submesoscale wavenumber spectra in drake passage. *J. Phys. Oceanogr.*, **46 (2)**, 601–620, doi:10.1175/JPO-D-15-0087.1.

Screen, J. A., N. P. Gillett, D. P. Stevens, G. J. Marshall, and H. K. Roscoe, 2009: The Role of Eddies in the Southern Ocean Temperature Response to the Southern Annular Mode. *Journal of Climate*, **22 (3)**, 806–818, doi:10.1175/2008JCLI2416.1.

Smedsrud, L., 2005: Warming of the deep water in the weddell sea along the greenwich meridian: 1977–2001. *Deep Sea Research Part I: Oceanographic Research Papers*, **52**, 241–258, doi:10.1016/j.dsr.2004.10.004.

St-Laurent, P., J. M. Klinck, and M. S. Dinniman, 2013: On the role of coastal troughs in the circulation of warm circumpolar deep water on antarctic shelves. *J. Phys. Oceanogr.*, **43 (1)**, 51–64, doi:10.1175/JPO-D-11-0237.1.

Stewart, A. L., A. Klocker, and D. Menemenlis, 2018: Circum-antarctic shoreward heat transport derived from an eddy- and tide-resolving simulation. *Geophys. Res. Lett.*, **45 (2)**, 834–845, doi:10.1002/2017GL075677.

Stewart, A. L., and A. F. Thompson, 2015: Eddy-mediated transport of warm circumpolar deep water across the antarctic shelf break. *Geophys. Res. Lett.*, **42 (2)**, 432–440, doi:10.1002/2014GL062281.

Stössel, A., D. Notz, F. A. Haumann, H. Haak, J. Jungclaus, and U. Mikolajewicz, 2015: Controlling high-latitude southern ocean convection in climate models. *Ocean Modell.*, **86**, 58 – 75, doi:https://doi.org/10.1016/j.ocemod.2014.11.008.

Stouffer, R. J., and Coauthors, 2006: Investigating the Causes of the Response of the Thermohaline Circulation to Past and Future Climate Changes. *Journal of Climate*, **19 (8)**, 1365–1387, doi:10.1175/JCLI3689.1.

Swart, N. C., and J. C. Fyfe, 2012: Observed and simulated changes in the southern hemisphere surface westerly wind-stress. *Geophysical Research Letters*, **39 (16)**, doi:10.1029/2012GL052810.

Taylor, K. E., R. J. Stouffer, and G. A. Meehl, 2012: An overview of cmip5 and the experiment design. *Bull. Amer. Meteor. Soc.*, **93 (4)**, 485–498, doi:10.1175/BAMS-D-11-00094.1.

Thompson, A., A. Stewart, P. Spence, and K. Heywood, 2018: The antarctic slope current in a changing climate. *Reviews of Geophysics*, **56**, doi:10.1029/2018RG000624.

Thompson, D., S. Solomon, P. Kushner, M. England, K. Grise, and D. Karoly, 2011: Signatures of the antarctic ozone hole in southern hemisphere surface climate change. *Nature Geoscience*, **4**, 741–749, doi:10.1038/ngeo1296.

Thompson, D. W. J., and S. Solomon, 2002: Interpretation of recent southern hemisphere climate change. *Science*, **296 (5569)**, 895–899, doi:10.1126/science.1069270.

Thompson, D. W. J., J. M. Wallace, and G. C. Hegerl, 2000: Annular modes in the extratropical circulation. part ii: Trends. *Journal of Climate*, **13 (5)**, 1018–1036, doi:10.1175/1520-0442(2000)013<1018:AMITEC>2.0.CO;2.

Weijer, W., M. E. Maltrud, M. W. Hecht, H. A. Dijkstra, and M. A. Kliphuis, 2012: Response of the Atlantic Ocean circulation to Greenland Ice Sheet melting in a strongly-eddying ocean model. *Geophysical Research Letters*, **39 (9)**, doi:10.1029/2012GL051611.

Whitworth, T., A. H. Orsi, S.-J. Kim, W. D. Nowlin Jr., and R. A. Locarnini, 2013: *Water Masses and Mixing Near the Antarctic Slope Front*, 1–27. American Geophysical Union (AGU), doi:10.1029/AR075p0001.

Winton, M., 2000: A reformulated three-layer sea ice model. *Journal of Atmospheric and Oceanic Technology*, **17 (4)**, 525–531, doi:10.1175/1520-0426(2000)017<0525:ARTLSI>2.0.CO;2.

Winton, M., W. G. Anderson, T. L. Delworth, S. M. Griffies, W. J. Hurlin, and A. Rosati, 2014: Has coarse ocean resolution biased simulations of transient climate sensitivity? *Geophysical Research Letters*, **41 (23)**, 8522–8529, doi:10.1002/2014GL061523.

Winton, M., R. Hallberg, and A. Gnanadesikan, 1998: Simulation of density-driven frictional downslope flow in z-coordinate ocean models. *J. Phys. Oceanogr.*, **28 (11)**, 2163–2174, doi:10.1175/1520-0485(1998)028<2163:SODDFD>2.0.CO;2.